Doctoral Dissertation

Study on Crack Propagation Behaviors of Double Network Hydrogels under High Stretch

（高延伸下におけるダブルネットワークゲルの

亀裂進展挙動に関する研究）

By

Ye Zhang

Supervisor: Jian Ping Gong

Laboratory of Soft & Wet Matter,

Graduate School of Life Science, Hokkaido University

Sapporo 001-0021, Japan

March, 2022

Contents

Chapter 1: General Introduction 3

1.1 Overview 3

1.2 Outline of this dissertation 5

1.3 Reference 8

Chapter 2: Background 13

2.1 Double network hydrogels 13

2.2 Fracture Mechanics 17

2.3 Crack Propagation Behaviors of Sort Materials 21

2.4 Reference 25

Chapter 3: Crack Propagation Behaviors of DN Gels ... 33

3.1 Introduction 33

3.2 Experiments 34

3.2.1 Materials 34

3.2.2 Gel synthesis 34

3.2.3 Uniaxial tensile test 37

3.2.4 Cyclic tensile test 37

3.2.5 Crack Growth Test with Real-Time Birefringence Image Observation 38

3.3 Results & discussions 41

3.3.1 Uniaxial tensile behavior 41

3.3.2 Cyclic tensile behavior 43

3.3.3 Crack growth behavior under tension 46

3.3.4 Real-time birefringence observation during crack growth 54

3.3.5 Velocity jump 58

3.3.6 Suppression of slow mode in necking DN gels 59

3.3.7 Crack growth behavior of DN gels with denser second network 61

3.4 Conclusions 66

3.5 Reference 67

Chapter 4: Crack Shapes of DN gels..... 71

4.1 Introduction 71

4.2 Experiments 72

4.2.1 Material & synthesis of DN gels 72

4.2.2 Mechanical properties of DN gels..... 73

4.2.3 Image analysis of crack shapes 74

4.3 Results & discussions 76

4.3.1 Characterization of crack shapes..... 76

4.3.2 Half CTOD length scale ℓ around crack tips 82

4.3.3 Relationship between ℓ and energy flux into propagating cracks 83

4.4 Conclusions 86

4.5 Reference..... 86

Chapter 5: Summary of the dissertation 90

List of Publications..... 92

Acknowledgement 95

Chapter 1: General Introduction

1.1 Overview

Hydrogels, which are composed of three-dimensional polymer network containing water as solvent, have attracted much attention as novel materials. These soft and wet materials show unique properties, such as flexibility, high water retention, low sliding friction [1], biocompatibility [2,3] and ability to exchange their components with surrounding environment, which hard and dry materials never show. Since these properties are useful in biological environment, hydrogel materials have been expected to be applied as biomaterials [4]. However, practical applications of hydrogel materials have been restricted because of their brittleness [5].

In the 21st century, various strategies to overcome this problem have been developed, which dramatically enhances the potential of hydrogel materials in load-bearing applications [6–10]. A brittleness of a typical synthetic hydrogel is mainly derived from the inhomogeneity of its network structure, which causes microscopic stress concentrations at microcracks where polymer network is locally sparse [5,11], and also derived from the insufficient polymer density, which gives the so low fracture energy that cracks can propagate easily [12,13]. Thus, the toughening strategies for hydrogels materials can be categorized in two types; one is designing an uniformized polymer structure, and the other is increasing the amount of energy dissipation. To achieve the former, Ito *et al*. developed slide-ring gels by introducing movable cross-linking points into the polymer network [6,14], and Sakai *et al*. succeeded in fabricating tetra-PEG gels consisting of tetra-arm polymers [9], both of which are designed to disperse the

local tension in the polymer chains and show high stretchability and purely elastic mechanical responses. The latter strategy has been accomplished by introducing relatively weak interactions excessively into the network structure, which contributes to enhancing the fracture energy of materials [8,10,15–17]. Such strategy was firstly established in our laboratory by creation of hydrogels consisting of two independent and asymmetric networks, which is named as double network (DN) concept [8,18].

The double network (DN) concept informs an effective approach for the fabrication of polymeric materials with outstanding mechanical strength and toughness [8,13,18]. A typical tough DN material comprises two interpenetrating polymer networks with contrasting mechanical properties. That is, one network is rigid and brittle, whereas the other network is soft and stretchable [8,18]. DN materials show significantly higher resistances to crack initiation and propagation than those of their individual components [18–20]. Synergistic effect of DN concept is related to the substantial internal fracture of the brittle network [17,21–24]. The rigid and brittle network bears the load; nevertheless, it breaks at relatively small deformations, and the load is transferred to the soft and stretchable network, which also deforms. Then, strain-hardening of the load-bearing soft network induces further fracture of the neighboring brittle network entangled with the soft network, thereby continuously expanding the “damage zone” [25]. This load transfer appears as a yielding-like phenomenon and a necking phenomenon during uniaxial tensile elongation [26,27]. During this process, a large amount of sacrificial fracture of covalent bonds can be generated in the brittle network, which results in large energy dissipation and considerably enhances the crack resistances

of DN materials.

For various potential applications of DN materials, a clarification of fracture behaviors at various deformation states is indispensable. Previous studies on the fractures of DN hydrogels have mainly focused on the investigation of crack propagation from a pre-notched crack under monotonic loading by tearing tests [19,20,28–32]. On the other hand, the resistance to post-notched cracks in highly tensioned states has been hardly investigated for the DN gels. This property is also very important because such cracks can be accidentally inserted onto the loaded state during the usage like punctures of automotive tires by sharp nails. Because an unnotched sample can be loaded to a substantially higher tension than that of a pre-notched sample, the examination of post-notched crack propagation behaviors on unnotched samples enables the observation of fracture behaviors under overstretched state at which the crack could be accelerated by releasing of excess amount of elastic energy. Previously, using strip samples in pure shear geometries, the crack propagation dynamics at various input stretching energy has been investigated for soft materials such as rubbers. Such studies confirmed the existence of fracture mode that only occurs under highly stretched state and provided new insights for the design of novel materials with great crack resistance. [33–35].

1.2 Outline of this dissertation

As described above, this dissertation aims to evaluate the crack resistance for post-notched cracks under highly stretched state and to elucidate the fracture mechanism of DN gels through the analysis of the crack propagation behaviors.

In **Chapter 2,** backgrounds of this study are summarized. Firstly, previous studies on the mechanical properties and the crack resistances of DN gels are reviewed. Next, fundamental knowledges about fracture mechanics of polymer materials are described, and methods to evaluate crack resistance are explained. Finally, current progresses of studies on propagation behaviors of post-notched cracks under high stretch of soft materials are reviewed.

In **Chapter 3**, we report unique crack propagation behaviors of DN gels and their mechanisms. we investigated the crack growth behaviors of DN gels in stretched states by inducing crack seeds into these gels under various degrees of tension. This examination enables the analysis of crack propagation for a wide range of bulk energy release rate G. The power-law relationship between G and crack growth velocity v was investigated for DN gels with different tensile behaviors. We found that for brittle and unnecking DN gels, the velocities changed from slow mode (quasi-stationary fracture) to fast mode (dynamic fracture) with an increase in G, similar to that of a single network gel; in contrast, for necking DN gels having higher crack resistances than those of the unnecking DN gels, only fast modes were observed once the G is above a threshold. Real-time birefringence observation reveals a large damage zone around the crack tip at G slightly lower than the threshold, while the damage zone is hardly observed at G higher than the threshold. The results indicate that, for the necking DN gels, crack initiation has a large energy barrier owing to the formation of the damage zone; once this barrier is overcome, the excess energy release accelerates the crack propagation and therefore the gels exhibit dynamic fracture.

In **Chapter 4**, we report a systematic study on crack shapes of DN gels. We investigated the crack shapes captured by the crack growth test conducted in **Chapter 3** for various DN gels with different network structures. Fitting analysis of each crack profile by power low relation of $x = ay^b$ where x and y are perpendicular and parallel direction to the stretch axis revealed that the nonparabolic crack parameter b lower than 2 was observed for all DN samples, which indicates that the crack blunting occurs during crack propagation in DN gels. The correlation between the magnitude of b and the strain-hardening behaviors after damaged was verified by comparing the cyclic unloading curves of each sample. From a and b, a half crack tip opening displacement (CTOD) length scale ℓ could be calculated and related with nonlinear elastic length scale, which suggests a strong nonlinear elasticity play a role not only at crack initiation but also in fast-mode crack propagation. We also discussed the energy balance during crack propagation by calculating an energetic measure G_ℓ from the shear moduli and ℓ, which implies that the energy consumption around crack tip might be dominated by elasticity for necking DN gels whereas viscoelasticity for unnecking DN gels.

Finally, in **Chapter 5**, the conclusion and prospective contributions of this study are summarized.

1.3 Reference

[1] Jian Ping Gong, T. Kurokawa, T. Narita, G. Kagata, Y. Osada, G. Nishimura, M. Kinjo, Synthesis of Hydrogels with Extremely Low Surface Friction, *J. Am. Chem. Soc.*, 123 (2001) 5582–5583.

[2] F. Islands, D. Survey, Industrial Research Associations: Some Taxation Problems, *Nature*, 185 (1960) 63–64.

[3] K. Y. Lee, D. J. Mooney, Hydrogels for Tissue Engineering, *Chem. Rev.*, 101 (2001) 1869–1879.

[4] A. S. Hoffman, Hydrogels Used for Biomedical Applications, *Adv. Drug Deliv. Rev.*, 54 (2002) 3–12.

[5] J. Bastide, L. Leibler, Large-Scale Heterogeneities in Randomly Cross-Linked Networks, *Macromolecules*, 21 (1988) 2647–2649.

[6] Y. Okumura, K. Ito, The Polyrotaxane Gel : A Topological Gel By, *Adv. Mater.*, 8656 (2001) 485–487.

[7] K. Haraguchi, T. Takehisa, Nanocomposite Hydrogels: AUnique Organic-Inorganic Network Structure with Extraordinary Mechanical, Optical, and Swelling/De-Swelling Properties, *Adv. Mater.*, No. 16 (2002) 1120–1124.

[8] J. P. Gong, Y. Katsuyama, T. Kurokawa, Y. Osada, Double-Network Hydrogels with Extremely High Mechanical Strength, *Adv. Mater.*, 15 (2003) 1155–1158.

[9] T. Sakai, T. Matsunaga, Y. Yamamoto, C. Ito, R. Yoshida, S. Suzuki, N. Sasaki, M. Shibayama, U. Il Chung, Design and Fabrication of a High-Strength Hydrogel with Ideally Homogeneous Network Structure from Tetrahedron-like Macromonomers, *Macromolecules*, 41 (2008) 5379–

5384.

[10] J.-Y. Sun, X. Zhao, W. R. K. Illeperuma, O. Chaudhuri, K. H. Oh, D. J. Mooney, J. J. Vlassak, Z. Suo, Highly Stretchable and Tough Hydrogels, *Nature*, 489 (2012) 133–136.

[11] H. Furukawa, K. Horie, R. Nozaki, M. Okada, Swelling-Induced Modulation of Static and Dynamic Fluctuations in Polyacrylamide Gels Observed by Scanning Microscopic Light Scattering, *Phys. Rev. E - Stat. Physics, Plasmas, Fluids, Relat. Interdiscip. Top.*, 68 (2003) 14.

[12] Y. Tanaka, K. Fukao, Y. Miyamoto, Fracture Energy of Gels, *Eur. Phys. J. E*, 3 (2000) 395–401.

[13] T. Nakajima, Generalization of the Sacrificial Bond Principle for Gel and Elastomer Toughening, *Polym. J.*, 49 (2017) 477–485.

[14] K. Ito, Novel Cross-Linking Concept of Polymer Network: Synthesis, Structure, and Properties of Slide-Ring Gels with Freely Movable Junctions, *Polym. J.*, 39 (2007) 489–499.

[15] M. A. Haque, T. Kurokawa, G. Kamita, J. P. Gong, Lamellar Bilayers as Reversible Sacrificial Bonds to Toughen Hydrogel: Hysteresis, Self-Recovery, Fatigue Resistance, and Crack Blunting, *Macromolecules*, 44 (2011) 8916–8924.

[16] T. L. Sun, T. Kurokawa, S. Kuroda, A. Bin Ihsan, T. Akasaki, K. Sato, T. Nakajima, J. P. Gong, M. A. Haque, T. Nakajima, J. P. Gong, M. A. Haque, Physical Hydrogels Composed of Polyampholytes Demonstrate High Toughness and Viscoelasticity, *Nat. Mater.*, 12 (2013) 932–937.

[17] E. Ducrot, Y. Chen, M. Bulters, R. P. Sijbesma, C. Creton, Toughening

Elastomers with Sacrificial Bonds and Watching Them Break, *Science*, 344 (2014) 186–189.

[18] J. P. Gong, Why Are Double Network Hydrogels so Tough?, *Soft Matter*, 6 (2010) 2583–2590.

[19] Y. Tanaka, R. Kuwabara, Y. H. Na, T. Kurokawa, J. P. Gong, Y. Osada, Determination of Fracture Energy of High Strength Double Network Hydrogels, *J. Phys. Chem. B*, 109 (2005) 11559–11562.

[20] Q. M. Yu, Y. Tanaka, H. Furukawa, T. Kurokawa, J. P. Gong, Direct Observation of Damage Zone around Crack Tips in Double-Network Gels, *Macromolecules*, 42 (2009) 3852–3855.

[21] R. E. Webber, C. Creton, H. R. Brown, J. P. Gong, Large Strain Hysteresis and Mullins Effect of Tough Double-Network Hydrogels, *Macromolecules*, 40 (2007) 2919–2927.

[22] T. Nakajima, T. Kurokawa, S. Ahmed, W. Wu, J. P. Gong, Characterization of Internal Fracture Process of Double Network Hydrogels under Uniaxial Elongation, *Soft Matter*, 9 (2013) 1955–1966.

[23] T. T. Mai, T. Matsuda, T. Nakajima, J. P. Gong, K. Urayama, Distinctive Characteristics of Internal Fracture in Tough Double Network Hydrogels Revealed by Various Modes of Stretching, *Macromolecules*, 51 (2018) 5245–5257.

[24] K. Fukao, T. Nakajima, T. Nonoyama, T. Kurokawa, T. Kawai, J. P. Gong, Effect of Relative Strength of Two Networks on the Internal Fracture Process of Double Network Hydrogels As Revealed by *in Situ* Small-Angle X-Ray Scattering, *Macromolecules*, 53 (2020) 1154–1163.

[25] Y. Tanaka, Y. Kawauchi, T. Kurokawa, H. Furukawa, T. Okajima, J. P. Gong, Localized Yielding around Crack Tips of Double-Network Gels, *Macromol. Rapid Commun.*, 29 (2008) 1514–1520.

[26] Y. H. Na, Y. Tanaka, Y. Kawauchi, H. Furukawa, T. Sumiyoshi, J. P. Gong, Y. Osada, Necking Phenomenon of Double-Network Gels, *Macromolecules*, 39 (2006) 4641–4645.

[27] T. Matsuda, T. Nakajima, Y. Fukuda, W. Hong, T. Sakai, T. Kurokawa, U. Il Chung, J. P. Gong, Yielding Criteria of Double Network Hydrogels, *Macromolecules*, 49 (2016) 1865–1872.

[28] S. Ahmed, T. Nakajima, T. Kurokawa, M. Anamul Haque, J. P. Gong, Brittle-Ductile Transition of Double Network Hydrogels: Mechanical Balance of Two Networks as the Key Factor, *Polymer*, 55 (2014) 914–923.

[29] T. Nakajima, H. Furukawa, Y. Tanaka, T. Kurokawa, Y. Osada, J. P. Gong, True Chemical Structure of Double Network Hydrogels, *Macromolecules*, 42 (2009) 2184–2189.

[30] S. Liang, J. Hu, Z. L. Wu, T. Kurokawa, J. P. Gong, Toughness Enhancement and Stick-Slip Tearing of Double-Network Hydrogels in Poly(Ethylene Glycol) Solution, *Macromolecules*, 45 (2012) 4758–4763.

[31] T. Nakajima, T. Kurokawa, H. Furukawa, J. P. Gong, Effect of the Constituent Networks of Double-Network Gels on Their Mechanical Properties and Energy Dissipation Process, *Soft Matter*, 16 (2020) 8618–8627.

[32] T. Matsuda, R. Kawakami, T. Nakajima, J. P. Gong, Crack Tip Field of a

Double-Network Gel: Visualizing Covalent Bond Scission by Mechanoradical Polymerization, *Macromolecules*, 53 (2020) 8787–8795.

[33] Y. Morishita, K. Tsunoda, K. Urayama, Velocity Transition in the Crack Growth Dynamics of Filled Elastomers: Contributions of Nonlinear Viscoelasticity, *Phys. Rev. E*, 93 (2016) 1–11.

[34] Y. Morishita, K. Tsunoda, K. Urayama, Crack-Tip Shape in the Crack-Growth Rate Transition of Filled Elastomers, *Polymer*, 108 (2017) 230–241.

[35] Y. Morishita, K. Tsunoda, K. Urayama, Universal Relation between Crack-Growth Dynamics and Viscoelasticity in Glass-Rubber Transition for Filled Elastomers, *Polymer*, 179 (2019) 121651.

Chapter 2: Background

2.1 Double network hydrogels

As described in **Chapter 1**, the DN concept is a novel toughening strategy for hydrogel materials. In this section, previous works about mechanical properties of DN gels are reviewed.

Initially, the DN concept were inspired by the structure of articular cartilages that show tremendously high compressive strengths while containing a large amount of water [1,2]. Articular cartilages are natural composite materials that are comprised of rigid proteoglycan and flexible collagen, which show high compressive fracture stress of 36 MPa [3,4]. Imitating it, the structure of DN gels is designed to consist of two polymer networks with contrasting mechanical properties. Typically, relatively sparse and tightly cross-linked polyelectrolyte is assigned as the first network while relatively dense and loosely cross-linked neutral polymer is assigned as the second network, and their interpenetrating structure are obtained by two-step UV polymerization method. Such strategy enables DN gels to exhibit extraordinary mechanical properties and to show unique fracture behaviors that cannot be observed in other materials.

One of the features of DN gels is yielding phenomena with necking behaviors [5,6]. Generally, some metal or plastic materials also show yielding of stress under uniaxial loading, but that of DN gels is quietly different from them. **Fig. 2-1a** shows a typical stress-strain curve of DN gels comprising poly(2-acrylamido-2-methylpropanesulfonic acid) (PAMPS) as the first network and poly(acrylamide) (PAAm) as the second network. Up to point A, the stress increases monotonically. However, the stress abruptly decreases at point B

accompanied by necking of sample as shown in **Fig. 2-1b**. Then, the stress keeps constant value until the necking zone expands to overall sample (point C), and the strain-hardening starts. During this process, the sacrificial bond breakages of the brittle first network and the load-transfer to the second network occur in the whole sample, which results in a large amount of energy dissipation. Actually, DN gels show great toughness of 10^7 J/m^3 in work of extension to fracture [1,7–9]. Ahmed *et al*. and Fukao *et al*. suggested that such toughness enhancement is contributed to load-transfer from the first network to the second network, which is governed by mechanical balance between the first network and the second network [9,10].

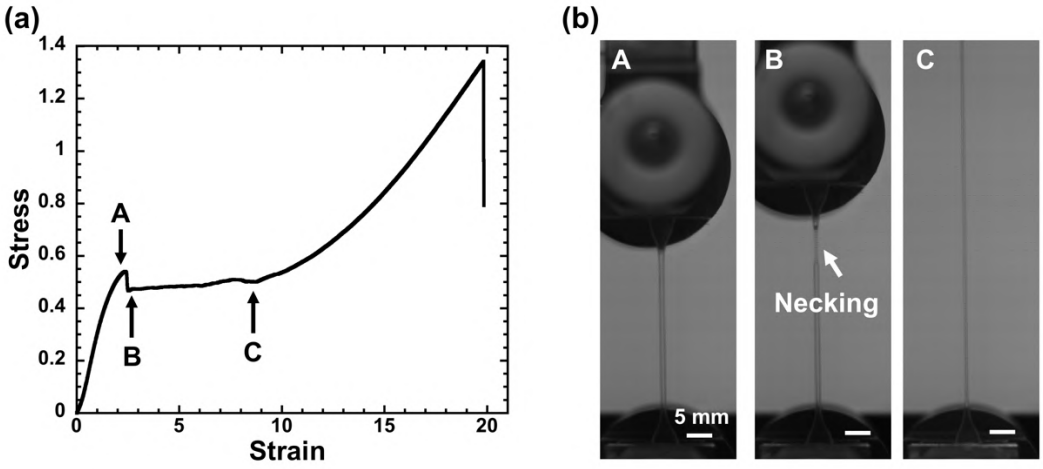

Fig. 2-1. (a) Stress–strain curve and (b) optical images of fracture behaviors of typical PMAPS/PAAm DN gels under uniaxial elongation.

Since the energy dissipation of DN gels is derived from chemical covalent bonds of the first network, DN gels show large hysteresis during cyclic loading process like Mullins effect observed in rubber materials [11,12]. Nakajima *et al*. verified that dissipated energy increase with an increase of strain, and approximately 85% of work of extension is dissipated at yielding points [8]. In

addition, it is confirmed that a decrease of elastic moduli from 0.25 MPa at virgin state to 0.038 MPa at end of the stress plateau region, and further decrease to 0.020 MPa at the hardening region. Since the value are close to the modulus of PAAm gels (0.018MPa), these results indicate that the first network break into fragments until yielding point and finally does not bear the load. They also demonstrated anisotropic reswelling along the pre-stretch direction, which suggests that preferential sacrificial bond breakage occurs only tensile direction until yielding points.

Such specific internal fracture of DN gels also can be observed as damage zone formation around crack tip [13–18]. Yu *et al*. reported that the damage zone in order of 100 μm was observed during tearing of DN gels by using a color 3D violet laser scanning microscope (**Fig. 2-2a**) [13]. Tanaka *et al*. verified the modulus softening of the damaged region by using atomic force microscope, which indicates the local yielding occurs at damage zone [19]. Recent works succeeded in more distinct visualization of damage zone by fluorescent probe for detection of bond breakage [17] and by birefringence observation [18] (**Figs. 2-2b and 2-2c**). The damage zone is assumed to contribute to the large fracture energy of DN gels, which are evaluated in order of 10^3 J/m^2 and comparable with that of rubber materials [7,9,12,20,21].

Subsequently, the DN concept was applied to various types of polymeric materials such as hydrogels [22–26], elastomers [16,27,28], and composite materials [29–31], which considerably expanded the possible application ranges of soft materials. Specifically, in addition to high strength, toughness, typical DN gels show high water retentions, low sliding frictions [32], biocompatibilities

[33,34], bond ability to bones [35] and fatigue resistance [36]. Therefore, DN gels have attracted significant attention as novel load-bearing biomaterials including artificial cartilages.

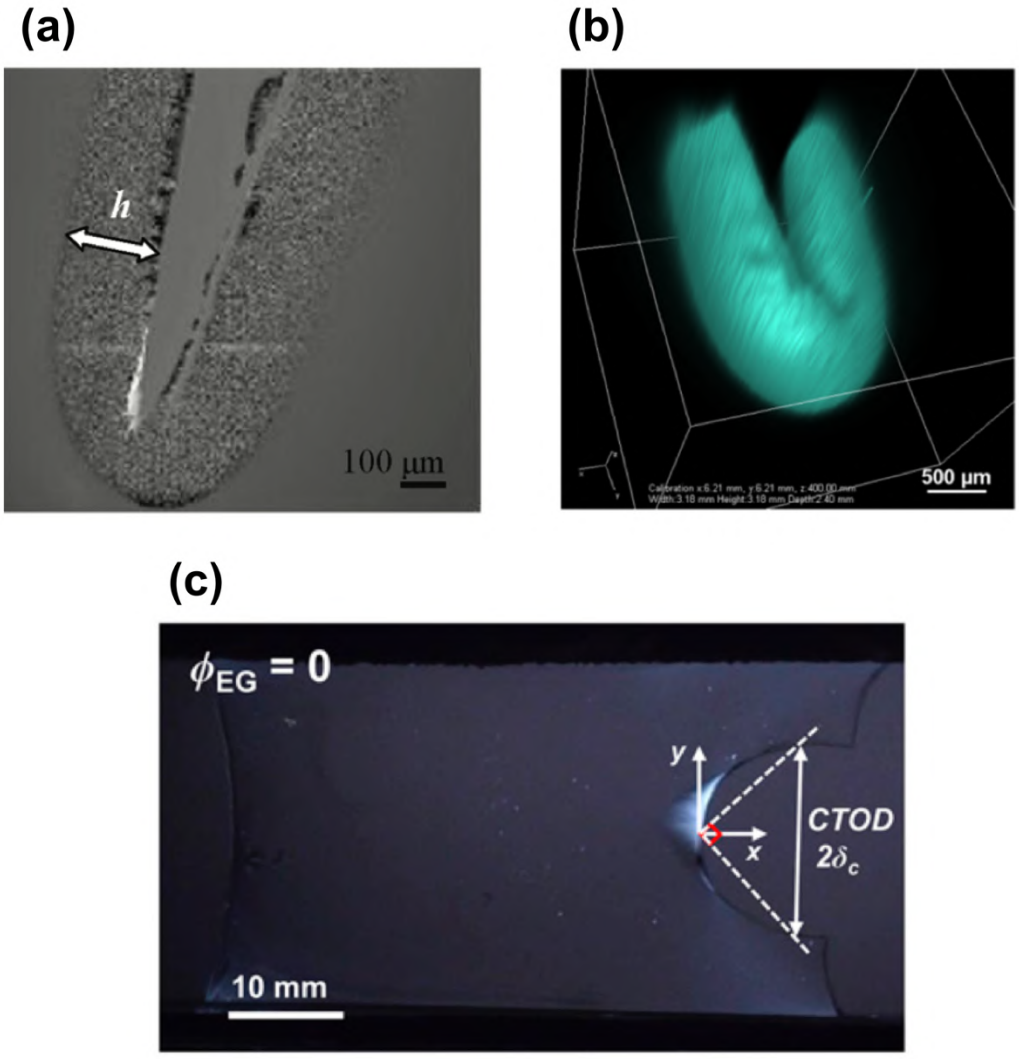

Fig. 2-2. Optical images of damage zone of DN gels (a) captured by using a color 3D violet laser scanning microscope after tearing [13], (b) obtained by the capture of the fluorescence 3D distribution where the mechanoradical polymerization of hydrophobic polymer is induced by the breakage of the first network [17], and (c) observed by birefringence measurement during pure shear test [18].

2.2 Fracture Mechanics

For applying as load-bearing biomaterials, the evaluation of the resistance to crack propagation of DN gels based on fracture mechanics is necessary. In this section, fundamental knowledges of fracture mechanics and methods to evaluate crack resistance are overviewed.

Generally, tensile tests and compression tests are widely used to characterize mechanical properties of materials. However, the criteria for fracture obtained by these tests, such as fracture stress and fracture strain, often shows variation. Furthermore, material sometimes breaks below these, which actually resulted in tragic accidents of a transport ship and a passenger airplane. This is because all materials contain small cracks and defects, and stress concentration occurs around them resulting in a start of crack propagations. Therefore, fracture mechanics has been developed to discuss fracture behavior based on the premise that crack exists in materials [37]. In the field of practical materials such as metals and rubbers, not only the estimation of the strength and lifetime, but also the elucidation of the fracture mechanism has been succeeded by focusing the crack propagation [38–40].

Thus, for applications of hydrogels, generally containing a lot of micro cracks due to inhomogeneous structures, their crack resistance should be measured. Commonly, the fracture energy of materials is regarded as the crack resistance. For a quasi-stationary crack advancing, the fracture energy Γ required is balanced by the strain energy released during crack extension [38,39]. Therefore, by measuring the strain energy released per unit area crack extension, called as the energy release rate G (J/m^2), the fracture energy Γ could be determined from the

relation $\Gamma = G$.

Rivlin and Thomas extended the theory of fracture mechanics for large deformable materials, which gives following definition of energy release rate G,

$$G = -\frac{1}{t}\left(\frac{\partial U}{\partial c}\right)_l \qquad (2.1)$$

where t is a thickness of samples, U is a stored elastic energy in the samples, and c is a crack length [38]. Energy release rate can be measured by following four experimental configurations: pure shear test, simple extension test, single edge crack test, and tearing test (**Fig. 2-3**). The simplest method for calculation of G is pure shear test (**Fig. 2-3a**), where G is given by

$$G = W(\varepsilon) \times l_0 \qquad (2.2)$$

where $W(\varepsilon)$ is a strain energy density in bulk at loaded to certain strain ε, and l_0 is an initial sample height. This equation can be easily derived as following explanation avoiding discussion about a complicated stress field around crack tips. Firstly, the specimen can be distinguished in four regions as shown in **Fig. 2-4** [41]. There are the region where strain energy is free (region I), that where the stress field and the strain field are quite complicated (region II), that where samples were purely under pure shear deformation (region III), and that where the stress field is affected by the edge (region IV). If the crack propagates in length of Δc, the region I broadens, and the region III narrows whereas the area of the region II and IV never change. Thus, the decreasing of stored elastic energy of samples can be described as

$$-dU = W\Delta chl_0 \qquad (2.3).$$

Combining this with equation (2.1) gives

$$G = -\frac{1}{h}\left(\frac{\partial U}{\partial c}\right)_{l} = W l_0 \qquad (2.4).$$

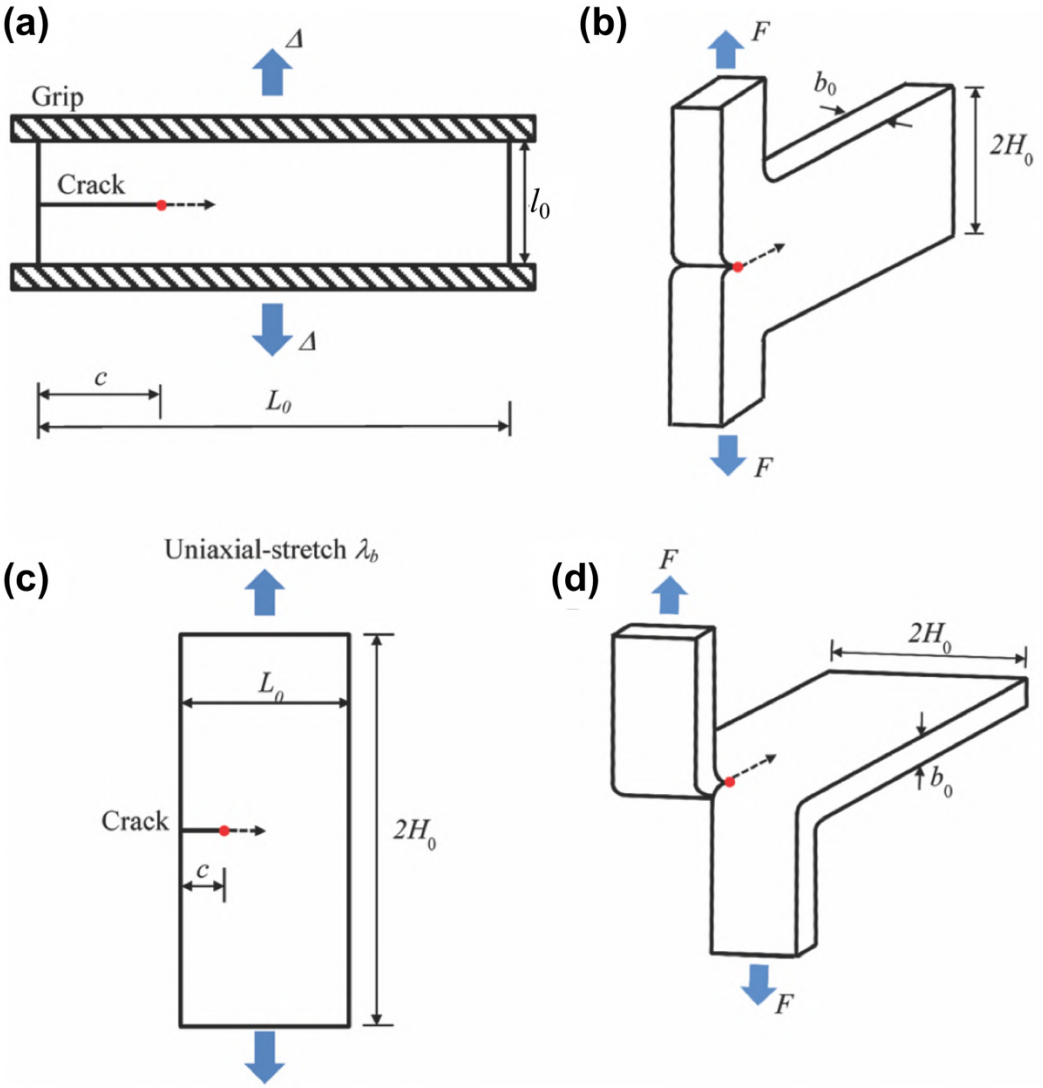

Fig. 2-3. Illustrations of experimental configurations for evaluation of fracture energy of soft materials [39]. (a) Pure shear test, (b) simple extension test, (c) single edge crack test, and (d) tearing test.

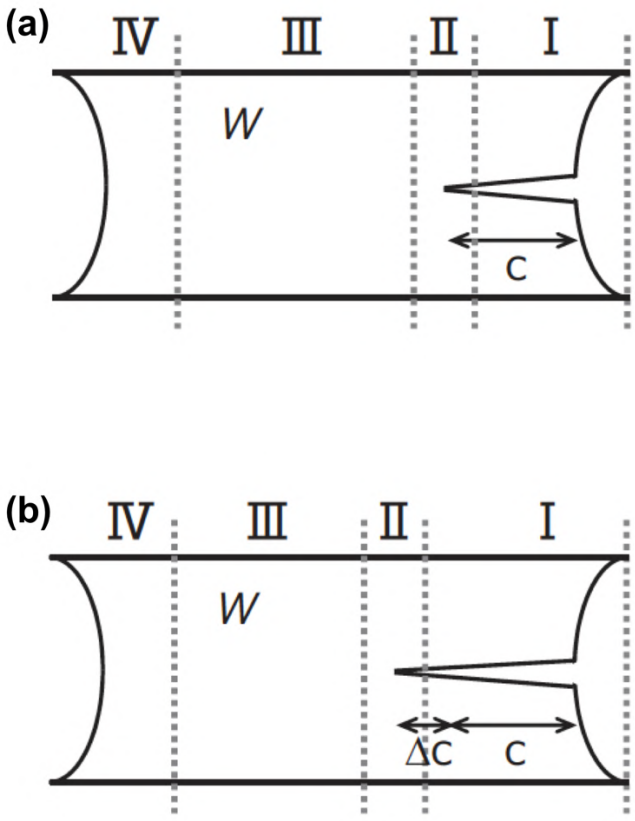

Fig. 2-4. Schematic illustration of crack propagation under pure shear deformation (a) before and (b) after crack propagates in Δc [41].

2.3 Crack Propagation Behaviors of Sort Materials

By using the methods described above, the fractur energies of several hydrogels have been evaluated. Conventional synthetic hydrogels such as PAAm gels show low fracture energy of 10^0–10^1 J/m^2 with rate-dependence [42–44]. On the other hand, DN gels show extraordinarily high fracture energy of 10^3 J/m^2 with rate-independence [20]. Since the fracture energy of PAMPS gels is estimated in 10^0 J/m^2 by Lake-Thomas theory [2,45], that of DN gels cannot be explained by a simple sum of those of two individual networks, which implies the synergetic effectivity of the DN concept.

However, most studies on fracture energy of DN gels were conducted only by the single edge crack test and the tearing test with large pre-notched cracks before loading. On the other hand, since a unnotched sample can be loaded to much higher tension than that of a pre-notched sample, this test enables to observe the fracture behaviors in a wide range of energy release rate. By investigating the power-law relationship between the energy release rate G and the velocity of post-notched crack propagation, it has been found that soft materials such as rubbers show slow mode (ductile fracture) at relatively low G, but the crack velocity abruptly jumps to fast mode (brittle fracture) at a critical energy release rate G_{jump} (**Fig. 2-5a**) [46,47]. From the perspective of application, the fast mode crack propagation may cause a catastrophic failure of materials resulting in serious accident of customers. Therefore, especially for practical materials, G_{jump} have been considered as new important material parameter for toughness. Morishita *et al*. found that the G_{jump} of styrene butadiene rubbers is affected by filler content, temperature and temperature [48]. Furthermore, it is demonstrated that G_{jump}

shows distinct correlation with the work of extensions normalized by the nonlinear elastic constant, which is independent on species of polymers and fillers [49]. Sakumichi *et al*. and Kubo *et al*. reported that rubbery-glassy transition of polymer network around crack tip causes the dramatic transition of crack propagation velocity by theoretical analysis and numerical calculation [50,51]. They also proposed strong correlation between G_{jump} and work of extension to fracture that depends on glass transition temperature of the materials, which will be helpful for designing new materials with greater crack resistances (**Fig. 2-5b**).

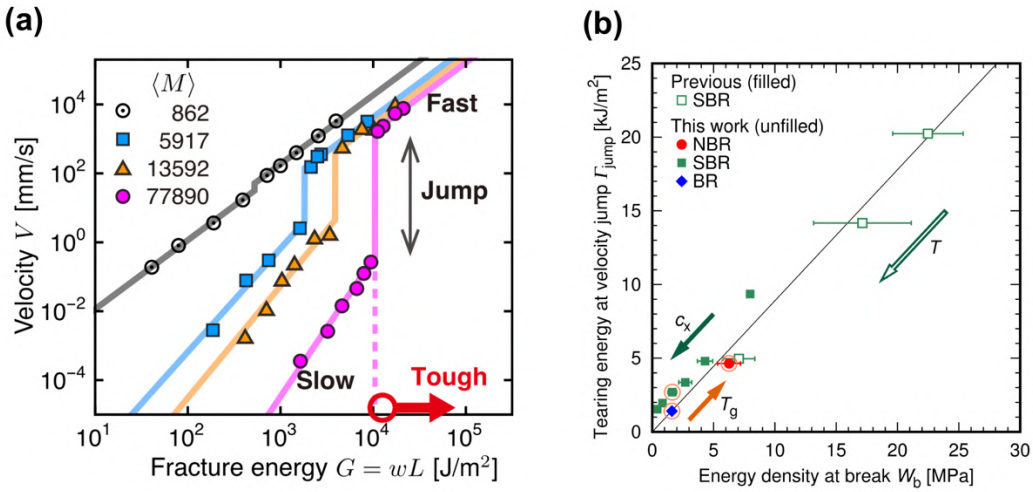

Fig. 2-5. (a) Logarithmic plots of the energy release rate G (denoted as fracture energy in [50]) and the velocity of crack growth v of styrene butadiene rubbers obtained by post-notching crack growth tests [46, 50] where M represents the average molar mass between cross-links. (b) Relationship between the work of extension to fracture W_{b} (denoted as energy density at break in [51]) and the critical energy release rate for velocity jump G_{jump} (denoted as tearing energy at velocity jump in [51]) of several species of elastomers. G_{jump} of the elastomers are strongly correlated with W_{b}, which is affected by cross-linker concentration, glass transition temperature, and environmental temperature.

For hydrogels, many works focusing on the post-notched cracks have been conducted since they show so slower crack propagation than other materials with high moduli that it is easy to observe shapes of propagating cracks [52–54]. Livne *et al*. demonstrated that the crack shapes of PAAm gels are different from a parabolic shape predicted by linear elastic fracture mechanics (LEFM) and sharpened owing to the strong nonlinearity around the crack tips during brittle fracture at which the crack velocity nearly reaches their shear wave speed (**Fig. 2-6**) [55]. Current study by Kolvin *et al*. revealed that the crack shape of tough DN gels significantly differs from other materials and obey a $x \sim y^{1.6}$ power law relation (**Fig. 2-7**) [56].

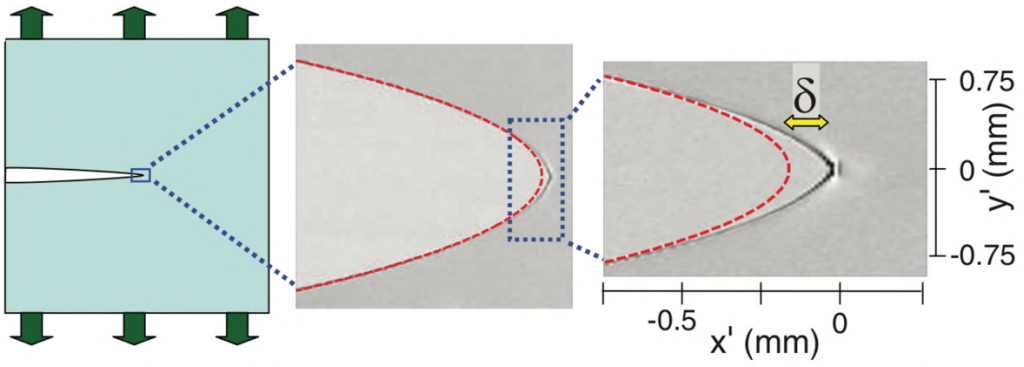

Fig. 2-6. (Left) Schematic illustration and (Center, Right) optical images of the shapes of the cracks of PAAm gels propagating in as high speed as their shear wave speed [55]. The crack shows deviations δ from the parabolic shape (red dashed line) predicted by LEFM.

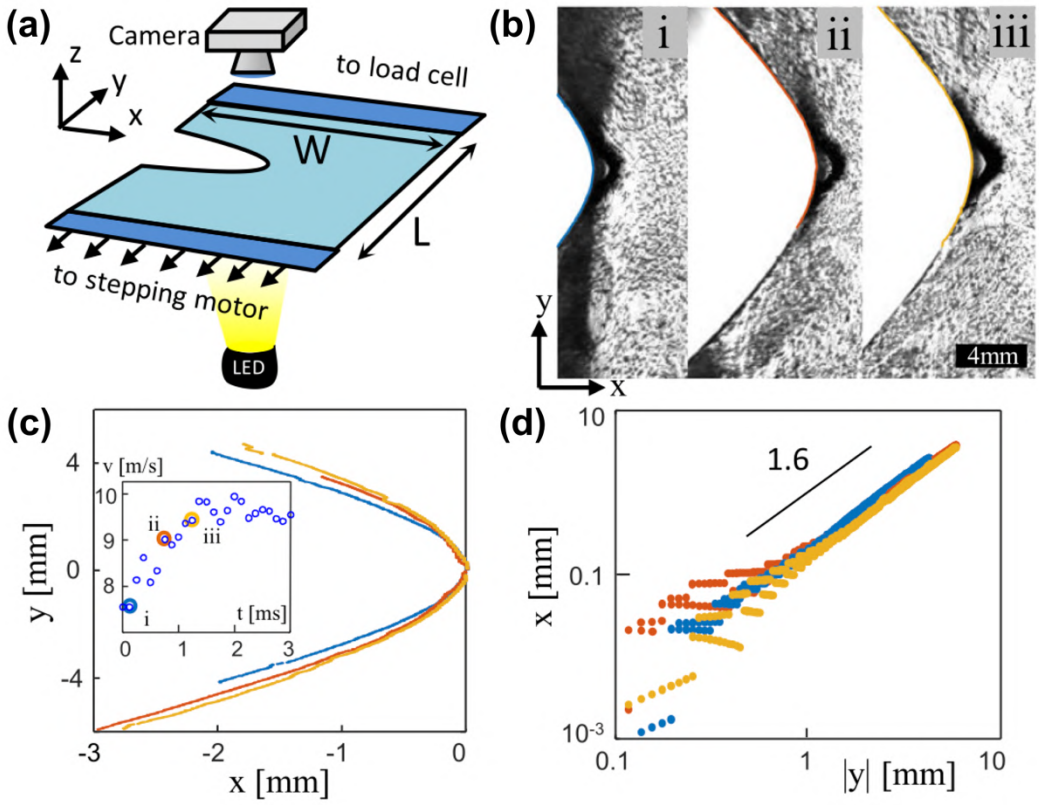

Fig. 2-7. (a) Schematic illustration of post-notching crack growth test of DN gels in [56]. (b) Optical images of the propagating cracks of DN gels. (c) Crack shape profiles extracted from each image where crack tip is set to the origin of axes. The inset image shows the relationship between time and the velocities of crack growth. (d) Logarithmic profiles of (c).

2.4 Reference

[1] J. P. Gong, Y. Katsuyama, T. Kurokawa, Y. Osada, Double-Network Hydrogels with Extremely High Mechanical Strength, *Adv. Mater.*, 15 (2003) 1155–1158.

[2] J. P. Gong, Why Are Double Network Hydrogels so Tough?, *Soft Matter*, 6 (2010) 2583–2590.

[3] A. J. Kerin, M. R. Wisnom, M. A. Adams, The Compressive Strength of Articular Cartilage, *Proc. Inst. Mech. Eng. Part H J. Eng. Med.*, 212 (1998) 273–280.

[4] N. K. Simha, C. S. Carlson, J. L. Lewis, Evaluation of Fracture Toughness of Cartilage by Micropenetration, *J. Mater. Sci. Mater. Med.*, 15 (2004) 631–639.

[5] Y. H. Na, Y. Tanaka, Y. Kawauchi, H. Furukawa, T. Sumiyoshi, J. P. Gong, Y. Osada, Necking Phenomenon of Double-Network Gels, *Macromolecules*, 39 (2006) 4641–4645.

[6] T. Matsuda, T. Nakajima, Y. Fukuda, W. Hong, T. Sakai, T. Kurokawa, U. Il Chung, J. P. Gong, Yielding Criteria of Double Network Hydrogels, *Macromolecules*, 49 (2016) 1865–1872.

[7] T. Nakajima, H. Furukawa, Y. Tanaka, T. Kurokawa, Y. Osada, J. P. Gong, True Chemical Structure of Double Network Hydrogels, *Macromolecules*, 42 (2009) 2184–2189.

[8] T. Nakajima, T. Kurokawa, S. Ahmed, W. Wu, J. P. Gong, Characterization of Internal Fracture Process of Double Network Hydrogels under Uniaxial Elongation, *Soft Matter*, 9 (2013) 1955–1966.

[9] S. Ahmed, T. Nakajima, T. Kurokawa, M. Anamul Haque, J. P. Gong, Brittle-Ductile Transition of Double Network Hydrogels: Mechanical Balance of Two Networks as the Key Factor, *Polymer*, 55 (2014) 914–923.

[10] K. Fukao, T. Nakajima, T. Nonoyama, T. Kurokawa, T. Kawai, J. P. Gong, Effect of Relative Strength of Two Networks on the Internal Fracture Process of Double Network Hydrogels As Revealed by *in Situ* Small-Angle X-Ray Scattering, *Macromolecules*, 53 (2020) 1154–1163.

[11] R. E. Webber, C. Creton, H. R. Brown, J. P. Gong, Large Strain Hysteresis and Mullins Effect of Tough Double-Network Hydrogels, *Macromolecules*, 40 (2007) 2919–2927.

[12] T. Nakajima, T. Kurokawa, H. Furukawa, J. P. Gong, Effect of the Constituent Networks of Double-Network Gels on Their Mechanical Properties and Energy Dissipation Process, *Soft Matter*, 16 (2020) 8618–8627.

[13] Q. M. Yu, Y. Tanaka, H. Furukawa, T. Kurokawa, J. P. Gong, Direct Observation of Damage Zone around Crack Tips in Double-Network Gels, *Macromolecules*, 42 (2009) 3852–3855.

[14] S. Liang, Z. L. Wu, J. Hu, T. Kurokawa, Q. M. Yu, J. P. Gong, Direct Observation on the Surface Fracture of Ultrathin Film Double-Network Hydrogels, *Macromolecules*, 44 (2011) 3016–3020.

[15] S. Liang, J. Hu, Z. L. Wu, T. Kurokawa, J. P. Gong, Toughness Enhancement and Stick-Slip Tearing of Double-Network Hydrogels in Poly(Ethylene Glycol) Solution, *Macromolecules*, 45 (2012) 4758–4763.

[16] E. Ducrot, Y. Chen, M. Bulters, R. P. Sijbesma, C. Creton, Toughening Elastomers with Sacrificial Bonds and Watching Them Break, *Science,* 344 (2014) 186–189.

[17] T. Matsuda, R. Kawakami, T. Nakajima, J. P. Gong, Crack Tip Field of a Double-Network Gel: Visualizing Covalent Bond Scission by Mechanoradical Polymerization, *Macromolecules*, 53 (2020) 8787–8795.

[18] Y. Zheng, T. Matsuda, T. Nakajima, W. Cui, Y. Zhang, C.-Y. Hui, T. Kurokawa, J. P. Gong, How Chain Dynamics Affects Crack Initiation in Double-Network Gels, *Proc. Natl. Acad. Sci.*, 118 (2021) e2111880118.

[19] Y. Tanaka, Y. Kawauchi, T. Kurokawa, H. Furukawa, T. Okajima, J. P. Gong, Localized Yielding around Crack Tips of Double-Network Gels, *Macromol. Rapid Commun.*, 29 (2008) 1514–1520.

[20] Y. Tanaka, R. Kuwabara, Y. H. Na, T. Kurokawa, J. P. Gong, Y. Osada, Determination of Fracture Energy of High Strength Double Network Hydrogels, *J. Phys. Chem. B*, 109 (2005) 11559–11562.

[21] T. Nakajima, H. Furukawa, Y. Tanaka, T. Kurokawa, J. P. Gong, Effect of Void Structure on the Toughness of Double Network Hydrogels, *J. Polym. Sci. Part B Polym. Phys.*, 49 (2011) 1246–1254.

[22] T. Nakajima, Generalization of the Sacrificial Bond Principle for Gel and Elastomer Toughening, *Polym. J.*, 49 (2017) 477–485.

[23] W. Yang, H. Furukawa, J. P. Gong, Highly Extensible Double-Network Gels with Self-Assembling Anisotropic Structure, *Adv. Mater.*, 20 (2008) 4499–4503.

[24] T. Nakajima, N. Takedomi, T. Kurokawa, H. Furukawa, J. P. Gong, A

Facile Method for Synthesizing Free-Shaped and Tough Double Network Hydrogels Using Physically Crosslinked Poly(Vinyl Alcohol) as an Internal Mold, *Polym. Chem.*, 1 (2010) 693–697.

[25] T. Nakajima, H. Sato, Y. Zhao, S. Kawahara, T. Kurokawa, K. Sugahara, J. P. Gong, A Universal Molecular Stent Method to Toughen Any Hydrogels Based on Double Network Concept, *Adv. Funct. Mater.*, 22 (2012) 4426–4432.

[26] J.-Y. Sun, X. Zhao, W. R. K. Illeperuma, O. Chaudhuri, K. H. Oh, D. J. Mooney, J. J. Vlassak, Z. Suo, Highly Stretchable and Tough Hydrogels, *Nature*, 489 (2012) 133–136.

[27] T. Matsuda, T. Nakajima, J. P. Gong, Fabrication of Tough and Stretchable Hybrid Double-Network Elastomers Using Ionic Dissociation of Polyelectrolyte in Nonaqueous Media, *Chem. Mater.*, 31 (2019) 3766–3776.

[28] Y. Zheng, R. Kiyama, T. Matsuda, K. Cui, X. Li, W. Cui, Y. Guo, T. Nakajima, T. Kurokawa, J. P. Gong, Nanophase Separation in Immiscible Double Network Elastomers Induces Synergetic Strengthening, Toughening, and Fatigue Resistance, *Chem. Mater.*, 33 (2021) 3321–3334.

[29] X. Feng, Z. Ma, J. V. MacArthur, C. J. Giuffre, A. F. Bastawros, W. Hong, A Highly Stretchable Double-Network Composite, *Soft Matter*, 12 (2016) 8999–9006.

[30] D. R. King, T. Okumura, R. Takahashi, T. Kurokawa, J. P. Gong, Macroscale Double Networks: Design Criteria for Optimizing Strength

and Toughness, *ACS Appl. Mater. Interfaces*, 11 (2019) 35343–35353.

[31] T. Okumura, R. Takahashi, K. Hagita, D. R. King, J. P. Gong, Improving the Strength and Toughness of Macroscale Double Networks by Exploiting Poisson's Ratio Mismatch, *Sci. Rep.*, 11 (2021) 1–13.

[32] D. Kaneko, T. Tada, T. Kurokawa, J. P. Gong, Y. Osada, Mechanically Strong Hydrogels with Ultra-Low Frictional Coefficients, *Adv. Mater.*, 17 (2005) 535–538.

[33] Y. Tanabe, K. Yasuda, C. Azuma, Y. Mei, C. Jian, J. P. Gong, Y. Osada, Biological Responses of Novel High-Toughness Double Network Hydrogels in Muscle and the Subcutaneous Tissues, *J. Mater. Sci. Mater. Med.*, 19 (2008) 1379–1387.

[34] K. Yasuda, N. Kitamura, J. P. Gong, K. Arakaki, H. J. Kwon, S. Onodera, Y. M. Chen, T. Kurokawa, F. Kanaya, Y. Ohmiya, Y. Osada, A Novel Double-Network Hydrogel Induces Spontaneous Articular Cartilage Regeneration *in Vivo* in a Large Osteochondral Defect, *Macromol. Biosci.*, 9 (2009) 307–316.

[35] T. Nonoyama, S. Wada, R. Kiyama, N. Kitamura, M. T. I. Mredha, X. Zhang, T. Kurokawa, T. Nakajima, Y. Takagi, K. Yasuda, J. P. Gong, Double-Network Hydrogels Strongly Bondable to Bones by Spontaneous Osteogenesis Penetration, *Adv. Mater.*, (2016) 6740–6745.

[36] W. Zhang, X. Liu, J. Wang, J. Tang, J. Hu, T. Lu, Z. Suo, Fatigue of Double-Network Hydrogels, *Eng. Fract. Mech.*, 187 (2018) 74–93.

[37] A. A. Griffith, The Phenomena of Rupture and Flow in Solids, *Philos. Trans. R. Soc. London. Ser. A, Contain. Pap. a Math. Phys. Character*,

221 (1921) 163–198.

[38] R. S. Rivlin, A. G. Thomas, Rupture of Rubber. I. Characteristic Energy for Tearing, *J. Polym. Sci.*, 10 (1953) 291–318.

[39] R. Long, C.-Y. Hui, Fracture Toughness of Hydrogels: Measurement and Interpretation, *Soft Matter*, 12 (2016) 8069–8086.

[40] R. Long, C. Y. Hui, J. P. Gong, E. Bouchbinder, The Fracture of Highly Deformable Soft Materials: A Tale of Two Length Scales, *Annu. Rev. Condens. Matter Phys.*, 12 (2021) 71–94.

[41] K. Tsunoda, Fracture Mechanics of Rubber, *J. Soc. Rubber Sci. Technol. Japan*, 87 (2014) 168–174.

[42] D. Bonn, H. Kellay, M. Prochnow, K. Ben-Djemiaa, J. Meunier, Delayed Fracture of an Inhomogeneous Soft Solid, *Science*, 280 (1998) 265–267.

[43] Y. Tanaka, K. Fukao, Y. Miyamoto, Fracture Energy of Gels, *Eur. Phys. J. E*, 3 (2000) 395–401.

[44] Y. Tanaka, R. Shimazaki, S. Yano, G. Yoshida, T. Yamaguchi, Solvent Effects on the Fracture of Chemically Crosslinked Gels, *Soft Matter*, 12 (2016) 8135–8142.

[45] G. J. Lake and A. G. Thomas, The Strength of Highly Elastic Materials, *Proc. Rolyal Soc. London. Ser. A, Math. Phys. Sci.*, (1967).

[46] K. Tsunoda, J. J. C. Busfield, C. K. L. Davies, A. G. Thomas, Effect of Materials Variables on the Tear Behaviour of a Non-Crystallizing Elastomer, *J. Mater. Sci.*, 35 (2000) 5187–5198.

[47] A. Takei, K. Okumura, Crack Propagation in Porous Polymer Sheets with Different Pore Sizes, *MRS Commun.*, 8 (2018) 1477–1482.

[48] Y. Morishita, K. Tsunoda, K. Urayama, Velocity Transition in the Crack Growth Dynamics of Filled Elastomers: Contributions of Nonlinear Viscoelasticity, *Phys. Rev. E*, 93 (2016) 1–11.

[49] Y. Morishita, K. Tsunoda, K. Urayama, Crack-Tip Shape in the Crack-Growth Rate Transition of Filled Elastomers, *Polymer*, 108 (2017) 230–241.

[50] N. Sakumichi, K. Okumura, Exactly Solvable Model for a Velocity Jump Observed in Crack Propagation in Viscoelastic Sheets, *Sci. Rep.*, 7 (2016) 1–11.

[51] A. Kubo, N. Sakumichi, Y. Morishita, K. Okumura, K. Tsunoda, K. Urayama, Y. Umeno, Dynamic Glass Transition Dramatically Accelerates Crack Propagation in Rubberlike Solids, *Phys. Rev. Mater.*, 5 (2021) 1–14.

[52] A. Livne, E. Bouchbinder, J. Fineberg, Breakdown of Linear Elastic Fracture Mechanics near the Tip of a Rapid Crack, *Phys. Rev. Lett.*, 101 (2008) 1–4.

[53] E. Bouchbinder, J. Fineberg, M. Marder, Dynamics of Simple Cracks, *Annu. Rev. Condens. Matter Phys.*, (2009) 371–397.

[54] T. Goldman Boué, R. Harpaz, J. Fineberg, E. Bouchbinder, Failing Softly: A Fracture Theory of Highly-Deformable Materials, *Soft Matter*, 11 (2015) 3812–3821.

[55] A. Livne, E. Bouchbinder, I. Svetlizky, J. Fineberg, The Near-Tip Fields of Fast Cracks, *Science*, 327 (2010) 1359–1363.

[56] I. Kolvin, J. M. Kolinski, J. P. Gong, J. Fineberg, How Supertough Gels

Break, *Phys. Rev. Lett.*, 121 (2018) 135501.

Chapter 3: Crack Propagation Behaviors of DN Gels [1]

"Reprinted from [1] Y.Zhang, K. Fukao, T. Matsuda, T. Nakajima, K. Tsunoda, T. Kurokawa, J. P. Gong, Unique crack propagation of double network hydrogels under high stretch, Extreme Mechanics Letters, 51 (2022) 101588, https://doi.org/10.1016/j.eml.2021.101588."

3.1 Introduction

As reviewed in **Chapter 2**, a lot of studies on crack propagation under various stretch have been reported, which enabled us to evaluate materials' crack resistances accurately for highly reliable designs of materials. Additionally, such works have expanded the possibilities of practical applications of materials and given many important insights to understand the fracture mechanism of materials. Additionally, as described in **Chapter 1**, the crack resistance for post-notches also should be evaluated for practical applications of DN materials

In this chapter, the study on crack propagation behaviors of DN gels is reported. The purpose of this study is elucidating the correlation between the double network structure and the crack growth behaviors at highly stretched state. We adopted DN hydrogels comprising the densely crosslinked polyelectrolyte poly(2-acrylamido-2-methylpropanesulfonic acid) (PAMPS) as the rigid and brittle network (first network) and the loosely crosslinked neutral polymer poly(acrylamide) (PAAm) as the soft and stretchable network (second network). We prepared DN gels with various network structures, which tuned their tensile behaviors from brittle to ductile. We analyzed the mode I crack growth behaviors of DN gels in stretched states by inducing crack seeds into these gels under various degrees of tension. We determined the power-law relationship between the strain

energy release rate of the bulk sample G and the crack growth velocity v at steady state. We performed real-time birefringence observation to characterize the damage zone of the samples around the crack tips. Finally, we analyzed the relationship between uniaxial tensile behaviors and crack growth behaviors and discussed the effect of the damage zone on the crack propagation behavior under tension.

3.2 Experiments

3.2.1 Materials

2-Acrylamido-2-methylpropanesulfonic acid (AMPS; Toa Gosei, Co., Ltd.) was used as received. Acrylamide (AAm; Junsei Chemical, Co., Ltd.) was recrystallized from acetone. *N*,*N*′-Methylenebisacrylamide (MBAA; FUJIFILM Wako Pure Chemical Corporation) and 2-oxoglutaric acid (α-keto; FUJIFILM Wako Pure Chemical Corporation) were used as received.

3.2.2 Gel synthesis

PAMPS/PAAm DN gels with the same first network compositions but different second network compositions were prepared (**Table 3-1**). DN gels consisting of PAMPS as the first network and PAAm as the second network were synthesized by the same procedures as previously reported [2]. The precursor PAMPS aqueous solution, containing 1 M AMPS as a monomer, 3 mol% MBAA as a crosslinker, and 1 mol% α-keto as an initiator (both relative to the monomer concentration), was poured into a glass mold consisting of two pieces of glass

plates separated by a 0.5 mm silicone rubber spacer. Then, the glass mold was irradiated with ultraviolet (UV) light for 6 h under an argon atmosphere for the synthesis of PAMPS gels by free-radical polymerization. The synthesized PAMPS gels were immersed in four different precursor PAAm aqueous solutions, containing AAm at different concentrations (0.8, 1.2, 1.6, and 2.0 M), 0.01 mol% MBAA, and 0.01 mol% α-keto (both relative to the monomer concentration), for at least 1 day until the PAMPS gels reached swelling equilibrium. Due to the osmotic pressure of the counter ions, the PAMPS gels considerably swelled, and the precursor PAAm aqueous solutions were incorporated into the PAMPS gels. Subsequently, the swollen PAMPS gels were sandwiched between two glass plates and irradiated with UV light for 8 h under an argon atmosphere for the synthesis of PAAm. A DN gel with a high crosslinker concentration of PAAm was also prepared from the precursor aqueous solution comprising 2.0 M AAm, 0.1 mol% MBAA, 0.01 mol% α-keto (both relative to the monomer concentration). The obtained DN gels were soaked in pure water for at least 3 days to remove unreacted reagents and to reach a new swelling equilibrium. The as-prepared DN gels only slightly swelled in pure water because PAMPS had already highly swelled in the precursor PAAm aqueous solutions, and the swelling of PAAm was suppressed by PAMPS. The thicknesses of the samples were slightly different because of different swelling ratios at equilibrium; however, the thicknesses of all the samples were in the range of 1.0–1.4 mm. The pre-stretch ratio of PAMPS in the swollen DN sample with respect to that of its as-prepared state, λ_s, is presented in **Table 3-1**. λ_s was estimated from the thickness of the swollen DN gel and the PAMPS gel during preparation (0.5 mm).

As reference samples, PAAm SN gels were also fabricated from an aqueous solution containing 2.0 M AAm, 0.01 mol% MBAA, and 0.01 mol% α-keto using a 1 mm thick silicone spacer. The PAAm gels were used in the as-prepared state without being swollen in water to maintain the SN concentration similar to that of the second network in the DN gel that hardly swelled after preparation.

For simplicity, DN gels were denoted as DN-C_2(-x_2), where C_2 (M) and x_2 (mol%) are the monomer concentration and the crosslinker concentration of the precursor PAAm aqueous solution. Unless otherwise stated, x_2 was 0.01 mol%. Similarly, the SN gels were represented as SN-C_2.

Table 3-1. A list of formulations and properties of the samples used in this study.

Sample code	Composition of the second network			λ_s [m/m]	Tensile behavior	$\lambda_s\lambda_y$ [m/m]	$\lambda_s^2\sigma_y$ [MPa]
	AAm C_2 [M]	MBAA x_2 [mol%]	α-keto [mol%]				
SN-C_2	2.0	0.01	0.01	−	Stretchable	−	−
DN-C_2(-x_2)	0.8	0.01	0.01	2.54 ± 0.04	Brittle	−	−
	1.2			2.45 ± 0.03	Necking	9.13 ± 0.15	3.79 ± 0.08
	1.6			2.50 ± 0.06	Necking	8.59 ± 0.21	3.60 ± 0.18
	2.0			2.69 ± 0.10	Necking	9.04 ± 0.33	3.93 ± 0.28
	2.0	0.1		2.39 ± 0.07	Unnecking	−	−

All the concentrations mentioned are the in-feed concentrations used in the precursor solutions. For DN gels, the first network formulations were the same, whereas the second network formulations were different. λ_s is the pre-stretch ratio of the first network in the DN gel. Tensile behaviors were characterized by the uniaxial stress–strain curves shown in **Fig. 3-4**. $\lambda_s\lambda_y$ and $\lambda_s^2\sigma_y$ are the stretch ratio and the nominal stress at yielding point normalized by λ_s, as shown in **Fig. 3-4**.

3.2.3 Uniaxial tensile test

Uniaxial tensile tests were conducted on samples cut into dumbbell shapes (gauge length: 12 mm and width: 2 mm) using a commercial tensile tester (Instron 5965, Instron Co.). The tensile velocity was fixed at 50 mm/min, corresponding to an initial strain rate of 0.07 s^{-1}. Young's moduli E of the gels were estimated from the initial slopes of the nominal stress (σ)–tensile strain (ε) curves in the strain range of 0.05–0.15.

3.2.4 Cyclic tensile test

As explained in Chapter 2, the energy release rate of the sample at preset strain $G(\varepsilon)$ was calculated from the σ–ε curves of unnotched samples with pure shear geometries as the notched samples by the following equation:

$$G(\varepsilon) = W_{el}(\varepsilon) \times l_0 \qquad (3.1)$$

where $W_{el}(\varepsilon)$ is the stored elastic strain energy density of the sample stretched to the strain ε and l_0 is the initial sample height [3,4]. For a purely elastic material, $W_{el}(\varepsilon)$ is determined from the area under the loading σ–ε curve. However, DN gels showed large mechanical hysteresis (Mullins effect) during the loading–unloading process, as schematically depicted in **Fig. 3-1**, because a certain amount of input energy was irreversibly dissipated by the fracture of the PAMPS network during sample stretching. The PAAm gel also demonstrated weak mechanical hysteresis due to the physical interaction between polymer chains. Therefore, the area under the unloading σ–ε curve $W_{unloading}(\varepsilon)$ can be taken as $W_{el}(\varepsilon)$ to calculate the G in this study. To obtain $G(\varepsilon)$, we conducted cyclic tensile tests of the samples in pure

shear geometries using a commercial tensile tester (Shimadzu Autograph AG-X universal tensile machine, Shimadzu Co.) at a tensile velocity of 50 mm/min. At first, the samples were loaded to a small strain of $\Delta\varepsilon$ and unloaded to the initial point. Then, the samples were loaded to $2\Delta\varepsilon$ and unloaded to the initial point. This process was repeated for n steps ($n = 1, 2, ...$) until the samples reached the yielding points or fractured. The area under the unloading curve of the step n under the maximum strain $\varepsilon_{\max,n} = n\Delta\varepsilon$ was evaluated as follows:

$$W_{\text{unloading},n}(\varepsilon_{\max,n}) = -\int_{\varepsilon_{\max,n}}^{0} \sigma_{\text{unloading}}(\varepsilon)\mathrm{d}\varepsilon \qquad (3.2).$$

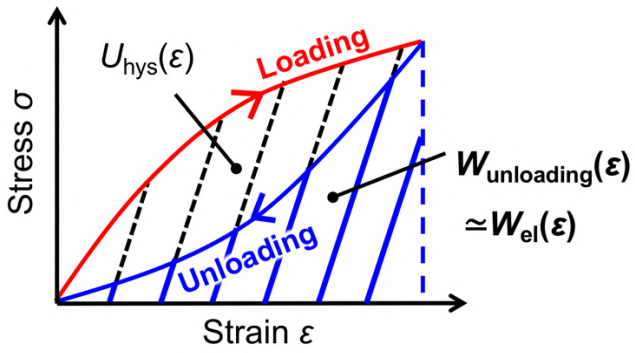

Fig. 3-1. Schematic illustration of stress–strain curves of the energy stored in typical DN gels. The red curve represents the loading stress–strain curve, and the blue curve depicts the unloading stress–strain curve. The black hatched area indicates the dissipated energy, U_{hys}, and the blue hatched area represents the stored strain energy of the fixed sample, W_{el}.

3.2.5 Crack Growth Test with Real-Time Birefringence Image Observation

Dynamic fracture tests of the samples in pure shear geometries were performed using the procedure schematically shown in **Fig. 3-2**. At first, the samples were clamped in rectangular shapes with 50 mm width and 10 mm initial height (l_0). Then, the samples were stretched to a preset strain at a tensile velocity

of 50 mm/min (Tensilon RTC-1150A, Orientec Co.). Thereafter, a ~10 mm long cut was created at one edge of the sample in the center using sharp scissors, and the crack propagation behaviors were observed by a polarized high-speed camera (CRYSTA PI-1P, Photron Co., Ltd.) [5]. The camera captured images at a rate of 3000 frames per second for short-term measurements or 60 frames per second for long-term measurements. From the acquired images, images showing crack propagation were extracted, and the time profiles of the crack length were obtained using ImageJ. For crack propagation in high-speed near shear wave speed (c_s), Goldman *et al*. demonstrated using a PAAm gel that crack acceleration becomes significantly sluggish at time $t \sim l_0/c_s$, owing to the interaction with the reflected elastic waves from the sample's vertical boundaries ("acquisition of inertia"), which results in the steady-state of v [6]. The cracks of our samples at fast speed also actually become approximately steady state within $l_0/c_s \sim 10^{-3}$–10^{-2} s as shown in Fig. S2 (l_0 = 10 mm and $c_s \sim$ 1–10 m/s). Therefore, v was estimated from the region where the crack propagated at a constant speed (**Fig. 3-3**). G as a function of the applied strain was estimated from the regression curves of $W_{\mathrm{unloading},n}(\varepsilon_{\mathrm{max},n})$ using equation (3.1). Simultaneously, to investigate molecular orientation around the cracks of DN gels, retardation R in each pixel of the images was also evaluated. Owing to the limitation of the measurement system, the discernible range of R was within 130 nm, corresponding to one-fourth of the light source wavelength (520 nm). The resolutions of the gray-scale images were approximately 80 μm/pixel, whereas those of the polarized light images were 160 μm/pixel. To avoid drying of samples in air, we set the maximum measurement times within ~100 seconds. Therefore, the minimum detection limit of v was ~10^{-6} m/s in this study.

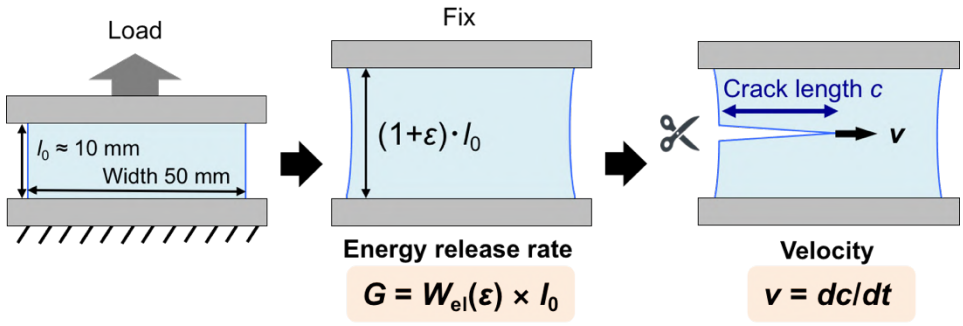

Fig. 3-2. (a) Schematics of crack growth test. Left: pure shear geometry of the test sample, middle: sample at stretching prior to notching, and right: crack propagation after notching.

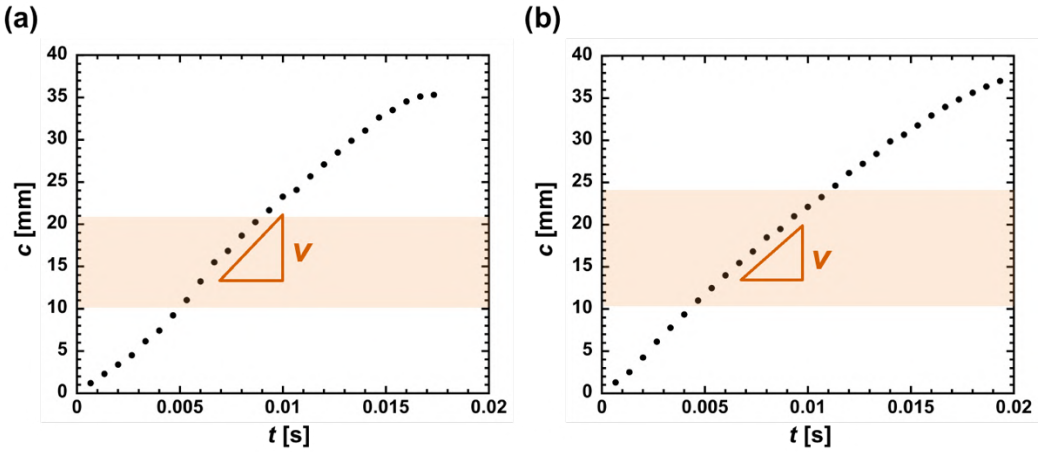

Fig. 3-3. Representative relationship between time t and cut length c during crack propagation in the case of (a) the fast-mode crack propagation of SN-2.0 ($G = 5.23 \times 10^2$ J/m^2, $v = 2.7$ m/s) and (b) the fast-mode crack propagation of DN-2.0 ($G = 1.63 \times 10^3$ J/m^2, $v = 2.0$ m/s). The crack growth velocity v was estimated from the region highlighted in orange where the crack propagated at a constant speed.

3.3 Results & discussions

3.3.1 Uniaxial tensile behavior

Figure 3-4 depicts the σ–ε curves of the SN and DN gels with different formulations measured by uniaxial tensile tests. Because the SN gel corresponding to the second network was loosely crosslinked, it was very stretchable; nevertheless, it broke at a relatively small stress. All the DN gels showed almost the same E because the first network compositions were nearly the same in these DN gels (**Table 3-2**). The DN gel with a low second network concentration (DN-0.8) easily fractured at a low fracture strain and low fracture stress, and this DN gel is defined as "brittle" DN gel hereinafter. In contrast, all the DN gels with high C_2 values (1.2–2.0 M) demonstrated yielding behaviors along with necking around the strain ε_y ~2.2, at which the stress quickly decreased initially and then plateaued. Thus, these samples are defined as "necking" DN gels hereinafter. The fracture strains of these necking DN gels increased with an increase in C_2; DN-1.2 fractured in the plateau region with a relatively low strain, whereas DN-1.6 and DN-2.0 showed distinct strain hardenings with large fracture strains.

As suggested in previous works, below the yielding point, internal fracture of the first network diffusively occurs, whereas above the yielding point, a large internal crack formed in the first network, and the second network strands, that may bridge the crack between the broken first network clusters, carry the load and are highly stretched [7,8]. Notably, the slightly different yielding points for the three necking DN gels are owing to the slightly different swellings of their first networks. After normalization by the pre-stretch ratio of the first network λ_s (**Table 3-1** and **Fig. 3-5**), the σ–ε curves and yielding points almost overlapped.

These results confirmed that below the yielding point, the mechanical behaviors of the DN gels are governed by the first network, irrespective of C_2 for the necking DN gels [9,10].

For the DN gel with a tightly crosslinked second network (DN-2.0-0.1), no abrupt decrease in stress and no plateau region were noticed, as indicated by the orange line in **Fig. 3-4**. The sample did not exhibit necking and a clear yielding point. Hereinafter, we denote this DN gel as "unnecking" DN gel.

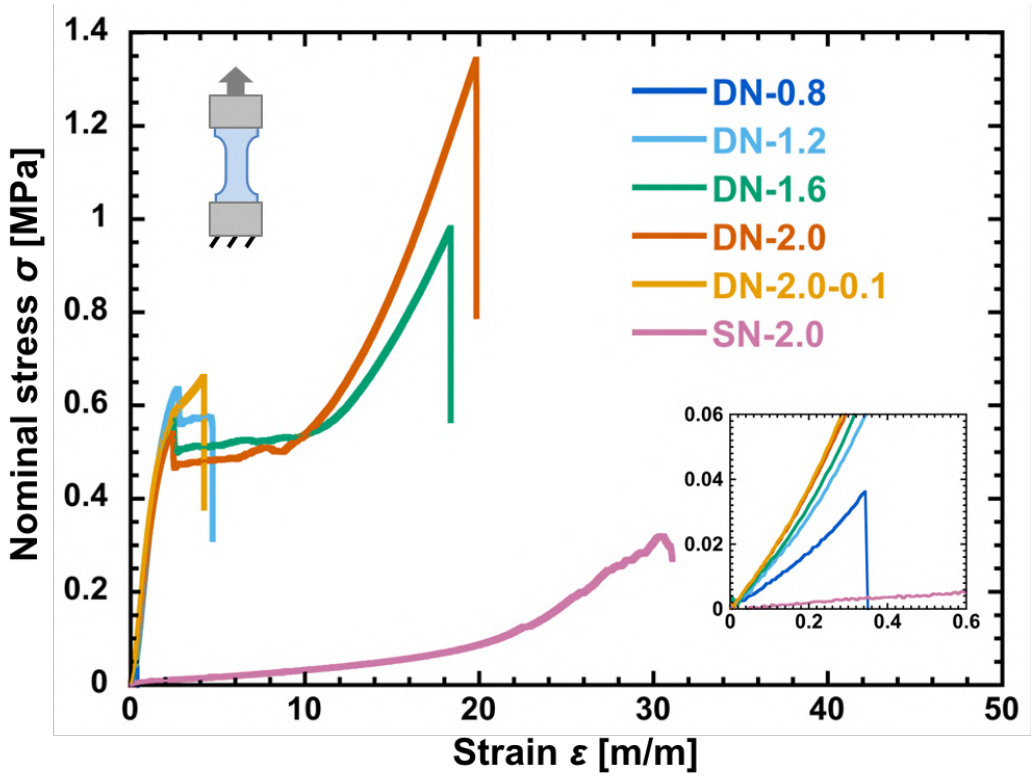

Fig. 3-4. Uniaxial tensile stress–strain curves of SN-2.0 and the DN gels with different concentrations of the second network and crosslinking densities. The inset shows the magnified stress–strain curves of brittle DN-0.8. The inset image depicts a schematic of the uniaxial tensile test. The sample codes are provided in **Table 3-1**.

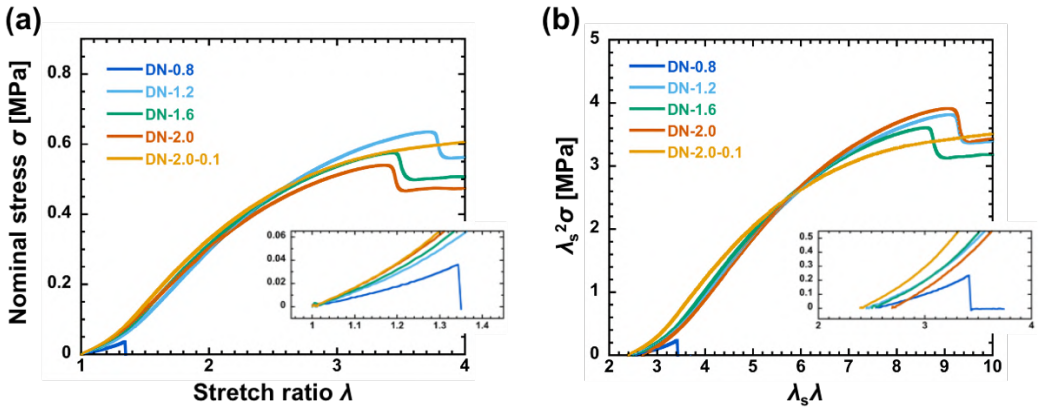

Fig. 3-5. (a) Uniaxial tensile stress–stretch ratio curves of all DN gels in relatively small stretching regimes. (b) Curves normalized by the pre-stretch ratio of the first network λ_s. The inset shows a magnified image of the curves of brittle DN-0.8.

3.3.2 Cyclic tensile behavior

Figure 3-6 shows the cyclic stress–strain curves of each sample. SN-2.0 and brittle DN-0.8 showed weak hysteresis. Necking and unnecking DN gels showed large hysteresis derived from the breakage of the sacrificial bonds. The relationships between $\varepsilon_{max,n}$ and $W_{unloading,n}$ ($\varepsilon_{max,n}$) for various samples is shown in **Figs. 3-7a** and **3-7b**. The $W_{unloading,n}$–$\varepsilon_{max,n}$ relations of SN-2.0 and brittle DN-0.8 were fitted by quadratic regression, whereas those of the other DN samples were fitted by linear regression. For necking DN gels, $U_{hys}/W_{loading,n}$ increased until yielding points and reached ~0.8, which are comparable with the results reported by previous work [7] (**Fig. 3-7d**).

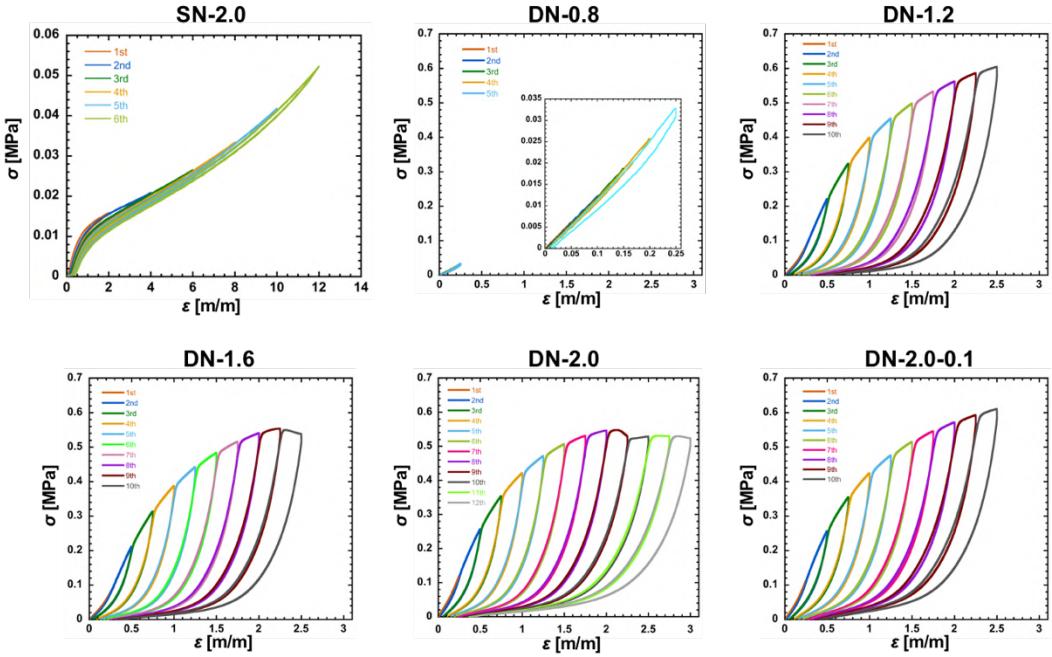

Fig. 3-6. Cyclic tensile stress–strain curves of the unnotched samples measured in pure shear geometries, as shown in **Fig. 3-2**. The strain ε (= $\varepsilon_{\max,n}$ = $n\Delta\varepsilon$) was increased stepwise with an increment ($\Delta\varepsilon$) from n = 1 to nth cycle. $\Delta\varepsilon$ = 2.0, n = 6 for SN-2.0, $\Delta\varepsilon$ = 0.05, n = 5 for brittle DN-0.8, $\Delta\varepsilon$ = 0.25, n = 12 for necking DN-2.0, and $\Delta\varepsilon$ = 0.25, n = 10 for other DN gels. The inset in the graph of brittle DN-0.8 shows magnified plots of the curves.

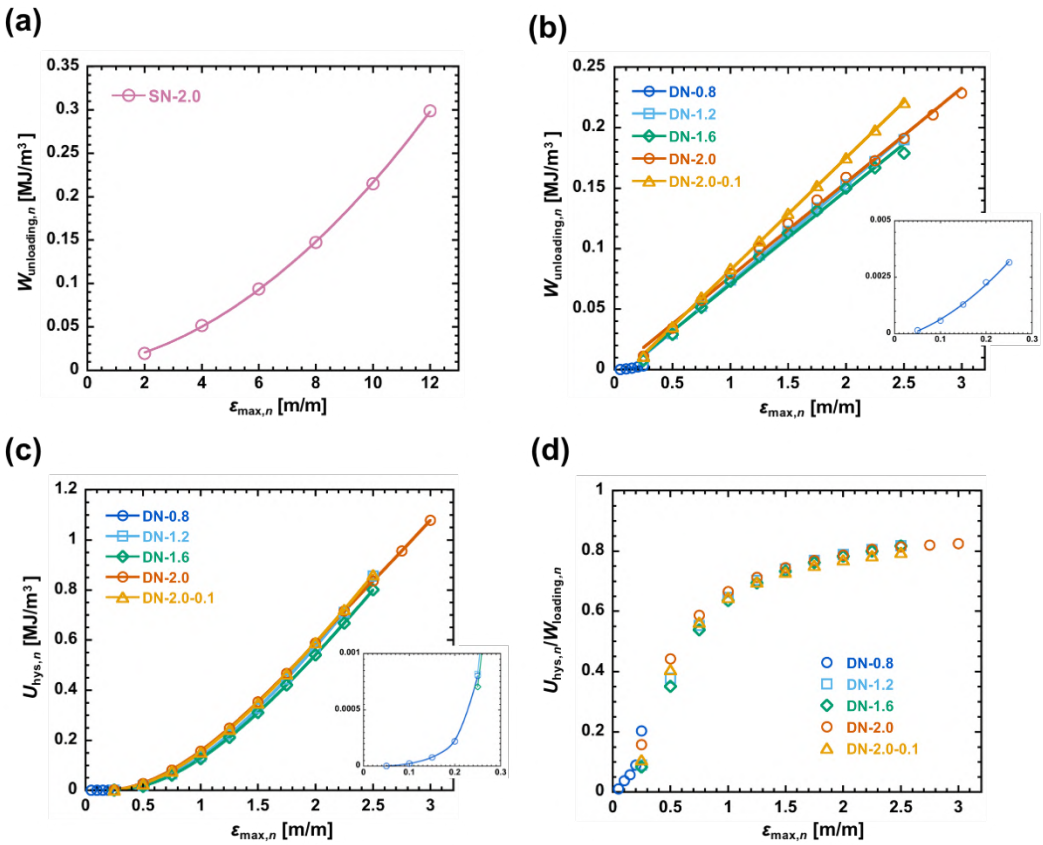

Fig. 3-7. (a) Dependence of $W_{unloading}$ on loading strain, $\varepsilon_{max,n}$, of SN-2.0. As the SN gel was loosely cross-linked, it showed a small amount of hysteresis (~5% to $W_{loading}$) due to rearrangement of polymer chains during loading. (b) Dependence of $W_{unloading}$ on $\varepsilon_{max,n}$ of all DN samples. The inset shows magnified plots of brittle DN-0.8. Brittle DN-0.8 that broke at a very small strain (~ 0.25) demonstrated a very weak mechanical hysteresis. In contrast, the $W_{unloading,n}$–$\varepsilon_{max,n}$ relations of necking and unnecking DN gels could be fitted by linear regression. (c) Dependence of dissipated energy, $U_{hys,n}$, on $\varepsilon_{max,n}$ of all DN samples. The inset shows magnified plots of brittle DN-0.8. (d) Dependence of ratio of the dissipated energy to the loading work, $U_{hys,n}/W_{loading,n}$, on $\varepsilon_{max,n}$ of all DN samples. Here, $U_{hys,n}$ and the loading work $W_{loading,n} = W_{unloading,n} + U_{hys,n}$ were calculated from **Fig. 3-6** in the same way as our previous work [7].

3.3.3 Crack growth behavior under tension

Figure 3-8 shows the optical images of the crack growth behavior, and **Fig. 3-9** depicts the power-law relationship between G and v for each sample. For SN-2.0, when the sample was cut at relatively low G, the crack propagated at very slow speeds (for example, $v = 2.4 \times 10^{-4}$ m/s at $G = 3.38 \times 10^{2}$ J/m^2, **Fig. 3-8a**). When the sample was cut at a relatively high G, the crack propagated at a very high speed (for example, $v = 2.7 \times 10^{0}$ m/s at $G = 9.35 \times 10^{2}$ J/m^2). From the G–v logarithmic plots of SN-2.0, the v jump was observed at a certain G (**Fig. 3-9a**). This phenomenon is similar to those noticed in the cases of filled elastomers [11,12], and we denote this critical value of energy release rate for velocity jump as G_{jump} in this study. For SN-2.0, the G_{jump} was approximately 4.5×10^{2} J/m^2, below which the crack propagated at very slow speeds ($v = 10^{-4}$–10^{-3} m/s), whereas, above which the cracks propagated at very high speeds ($v = 10^{0}$–10^{1} m/s).

Brittle DN-0.8 also demonstrated the v jump phenomenon but at a much lower G_{jump} ($\approx 6.0 \times 10^{1}$ J/m^2) than that of SN-2.0, below which the crack propagated at very slow speeds ($v = 10^{-3}$–10^{-2} m/s), whereas above G_{jump}, the crack propagated at very high speeds ($v > 10^{0}$ m/s; **Fig. 3-8b**). As DN-0.8 was too brittle to load to large G reproducibly, its fast-mode crack propagations only could be measured in low frame rate; nevertheless, we confirmed that v was at least more than 1.1×10^{0} m/s at $G = 6.29 \times 10^{1}$ J/m^2.

Unexpectedly, the necking DN gels showed unique crack propagation behaviors. As shown in **Fig. 3-8c**, the cracks in these samples did not propagate even at relatively large G values. However, the cracks started to propagate at very fast speeds ($v = 10^{0}$–10^{1} m/s) once G reached a threshold (denoted as G_{th},

hereinafter) of approximately 1.6×10^3 J/m^2 for DN-2.0, and slow speed crack propagation was not observed (**Figs. 3-9a** and **3-9b**). We verified that the necking DN gels could suppress crack propagation even with a large notch (approximately 10 mm) under high tension. For example, in the case of DN-2.0, the crack did not propagate at $\varepsilon \leq 2.3$, $\sigma \leq 0.52$ MPa, and $G \leq 1.55 \times 10^3$ J/m^2. We verified that the crack propagation could not be observed below G_{th} at least for 100 seconds, when the effect of sample drying in air was assumed to be negligible. As shown in **Table 3-2**, G_{th} of the necking DN gels slightly increased with an increase in C_2. In contrast, unnecking DN-2.0-0.1 with almost the same C_2 but a higher crosslinking density demonstrated a slow-mode crack propagation ($v = 10^{-5}$–10^{-3} m/s; **Fig. 3-8d**), and the slow-mode crack propagation switched to the fast-mode crack propagation at $G_{jump} \approx 1.35 \times 10^3$ J/m^2 (**Fig. 3-9a**). G_{jump} of the unnecking DN-2.0-0.1 is slightly lower than G_{th} of the corresponding necking DN-2.0.

Because the maximum crack propagation speed is limited by the shear wave speed (c_s) of materials, we normalized the v by $c_s = \sqrt{\mu/\rho}$, where μ is the shear modulus of the virgin samples and ρ is the mass density of the gels (**Table 3-2**). As shown in **Fig. 3-9c**, all v in the fast-mode region converge when normalized by their corresponding c_s, and v/c_s lies in the 0.1–1 range, which means that v in the fast mode approaches its maximum value.

In the slow-mode region where v is considerably lower than the shear wave velocity, the crack growth is in a quasi-stationary state with negligible inertia effect, and G is balanced by the rate-dependent fracture energy $\Gamma(v)$, namely, $\Gamma(v) = G$. According to the positive G dependence of v as shown in **Fig. 3-9a**, $\Gamma(v)$ slightly increases with v in the slow-mode region.

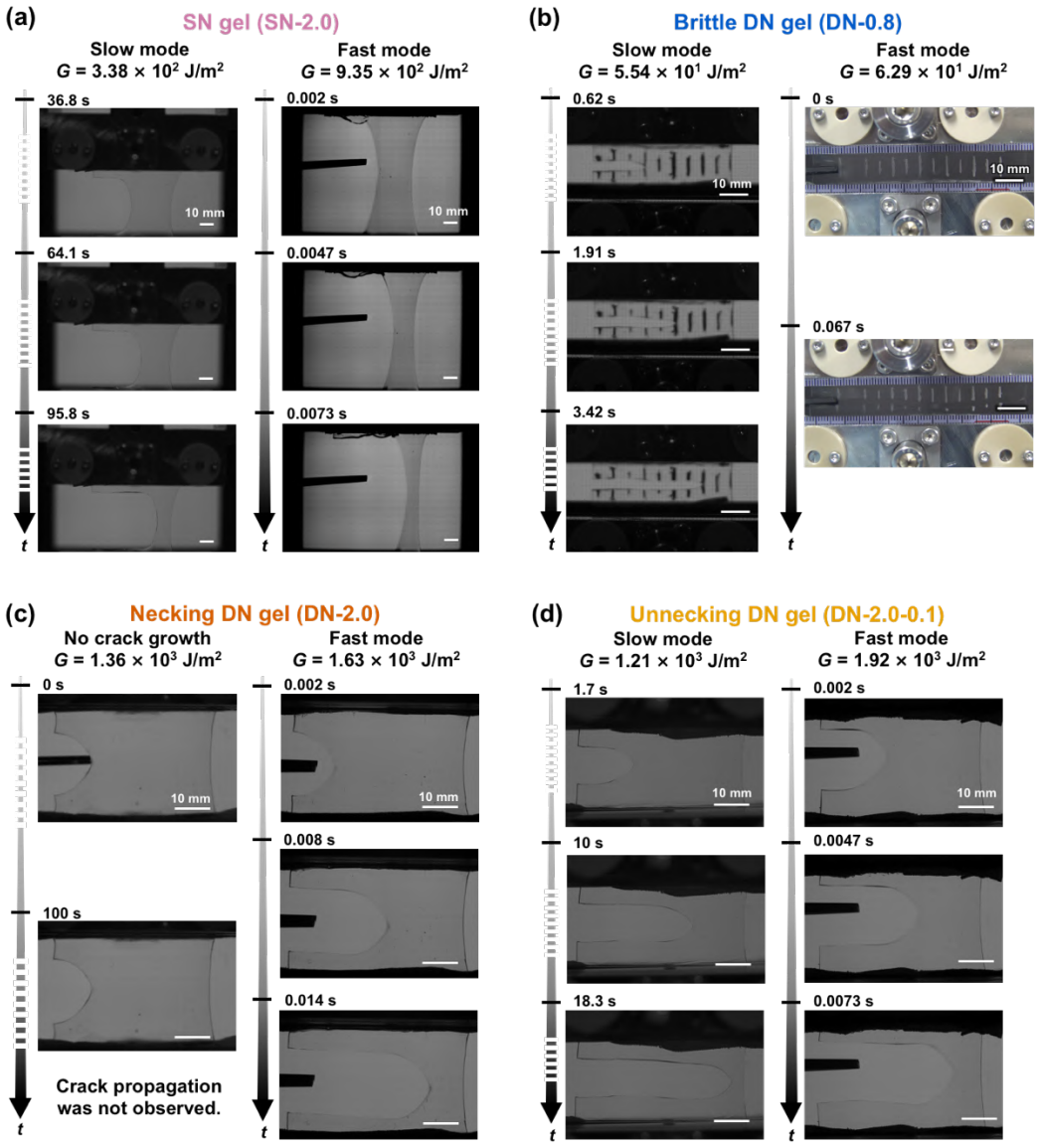

Fig. 3-8. Representative optical images showing the crack growth behaviors of (a) SN-2.0, (b) DN-0.8, (c) DN-2.0, and (d) DN-2.0-0.1. Scale bars represent 10 mm.

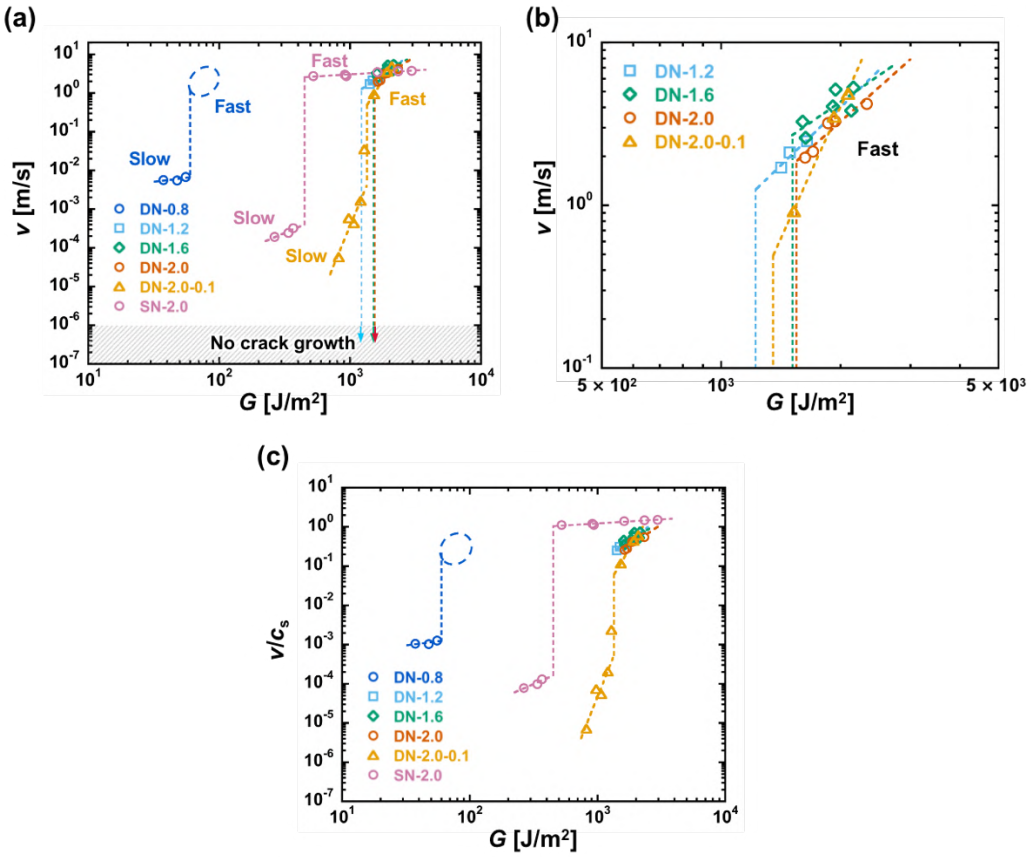

Fig. 3-9. (a) Logarithmic plots of the energy release rate G and the velocity of crack growth v measured by post-notch crack growth tests. The arrows depict the G at which crack propagation was not detected. The grey hatched regime indicates the crack propagation was not observed within experimental resolution (10^{-6} m/s). (b) Magnified images of the plots shown in (a) for the necking DN gels and unnecking DN-2.0-0.1 in the fast mode. (c) Logarithmic plots of G and v normalized by the shear wave speed c_s. The blue dashed circles in (a) and (c) represent the uncertainty of the crack velocity of DN-0.8 in the fast mode ($v > 1.1 \times 10^0$ m/s at $G = 6.29 \times 10^1$ J/m^2).

Table 3-2. A list of parameters related to crack propagation in the fast mode for the samples shown in **Table 3-1**.

Sample code	E [MPa]	c_s [m/s]	G_{jump} [J/m^2]	G_{th} [J/m^2]
SN-2.0	0.018 ± 0.006	2.4	≈ 4.5 × 10^2	−
DN-0.8	0.085 ± 0.004	5.3	≈ 6.0 × 10^1	−
DN-1.2	0.136 ± 0.013	6.7	−	≈ 1.3 × 10^3
DN-1.6	0.158 ± 0.007	7.3	−	≈ 1.55 × 10^3
DN-2.0	0.174 ± 0.005	7.6	−	≈ 1.6 × 10^3
DN-2.0-0.1	0.187 ± 0.008	7.9	≈ 1.35 × 10^3	−

E is the Young's moduli. c_s is the shear wave speed. $c_s = \sqrt{\mu/\rho}$ is calculated from the mass densities $\rho \approx 1$ g/cm^3 and the E by using the Poisson's ratio $\nu = 0.5$ and the shear modulus $\mu = E/2(1 + \nu) = E/3$ owing to the incompressibility of gels. For DN gels, E values of the virgin samples were used. G_{jump} is the critical value for the velocity jump from slow mode to fast mode of SN, brittle and unnecking DN gels, and G_{th} is the threshold value for the crack propagation of necking DN gels.

As G_{th} is the bulk energy release rate calculated from $G_{th} = W_{el}(\varepsilon_{th})l_0$, where ε_{th} is the critical strain for crack propagation at a certain initial sample height l_0, if G_{th} is the intrinsic critical G related to the crack propagation, it should not change with l_0. To confirm this, crack growth tests were performed on DN-2.0 with different l_0 (5, 8, and 15 mm) at a fixed sample width (50 mm). As shown in **Fig. 3-10**, the ε-v plots strongly depended on l_0 and the ε_{th} decreased with an increase in l_0, whereas the G-v plots almost collapsed on a master curve and the G_{th} hardly changed with an increase in l_0. This result verified that G_{th} is an intrinsic parameter, whereas ε_{th} is not. G_{th} is balanced with Γ_c, the energy dissipation for crack initiation, namely, $G_{th} = \Gamma_c$. It should be noted that the samples with smaller

l_0 have larger ε_{th} and therefore larger amount of brittle network in the DN samples has already broken during the loading process, as revealed by the large mechanical hysteresis of the loading-unloading curves in **Figs. 3-6** and **3-7**. However, we noticed that G_{th} and the G-v plots are hardly affected by l_0, which indicates that the breakage of the sacrificial network in the bulk during the loading process does not have a substantial impact on the crack initiation and propagation.

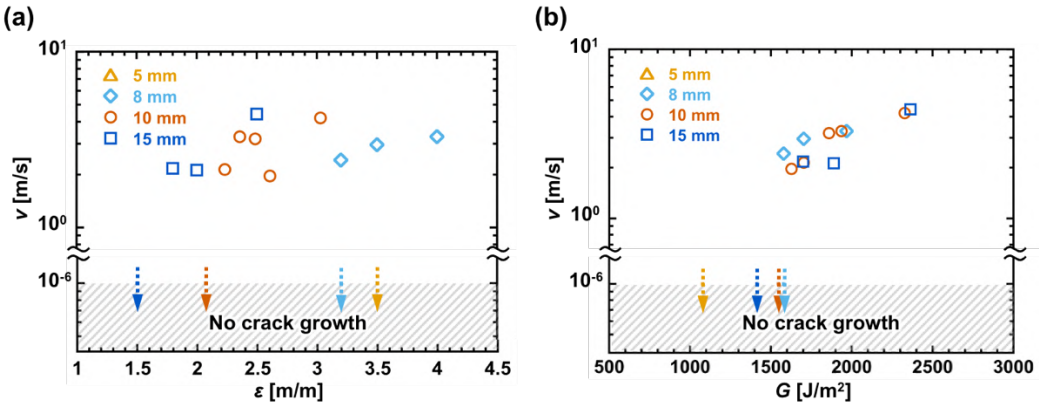

Fig. 3-10. The effect of initial sample height l_0 on the crack propagation of the necking DN gel (DN-2.0). (a) Crack velocity as a function of strain ε and (b) crack velocity as a function of the energy release rate G. The arrows depict the G at which crack propagation was not detected. The grey hatched regime indicates the crack propagation was not observed within experimental resolution. For the samples with smaller l_0 (= 5 and 8 mm), G at high ε (> 3) were calculated by the extrapolation of its $W_{unloading,n}$–$\varepsilon_{max,n}$ relation as shown in **Fig. 3-11**.

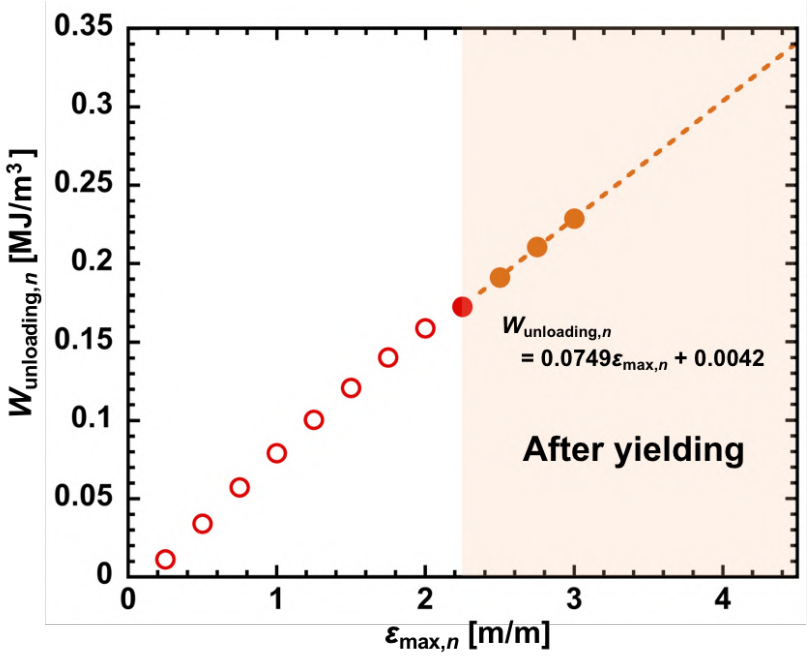

Fig. 3-11. Extrapolation of the $W_{unloading,n}$–$\varepsilon_{max,n}$ relation of DN-2.0 for the calculation of the G of samples with smaller l_0 under large preset strain ε (> 3) in **Fig. 3-10**. Our previous work demonstrated that, for a typical DN hydrogel, $U_{hys,n}/W_{loading,n}$ keeps constant after yielding point during cyclic tensile test [7]. If we assumed that $W_{loading,n}$ linearly increases with $\varepsilon_{max,n}$ after yielding, where the stress–strain curve shows plateau region, $W_{unloading,n} = W_{loading,n} - U_{hys} = W_{loading,n}(1 - U_{hys,n}/W_{loading,n})$ also should linearly increase with $\varepsilon_{max,n}$. Therefore, $W_{unloading}(\varepsilon)$ at large ε could be obtained by extrapolating the $W_{unloading,n}$–$\varepsilon_{max,n}$ relation in the after-yielding region ($\varepsilon_y \sim 2.25$ as shown in **Fig. 3-6**).

The above results indicate that for the necking DN gel, crack propagated above a large threshold energy release rate in fast mode. To determine whether the necking with yielding in the uniaxial tensile test and suppression of the slow-mode crack propagation were intrinsically correlated for DN gels with various structures, we further studied the behaviors of three DN gels with different first network composition (**Table 3-3**). **Fig. 3-12** shows the tensile properties and crack propagation behaviors of the three DN gels. For comparison, the results of other previously discussed DN gels are also presented. All samples can be classified into two groups: DN gels showing necking and yielding behaviors in the σ–ε curves and DN gels only exhibiting certain strain softening but no necking (**Fig. 3-12a**). Again, as shown in **Fig. 3-12b**, all the necking samples did not demonstrate slow-mode crack propagation, whereas all the unnecking samples showed slow-mode crack propagation. Although no significant differences were noticed between the tensile fracture stresses of DN-1.2 and DN-2.0-0.1, and between DN-N2 and DN-U1, depending on whether necking and yielding occurred or not, considerable differences were observed between the crack propagation behaviors of DN-1.2 and DN-2.0-0.1, and between those of DN-N2 and DN-U1.

Table 3-3. A list of formulations and the existence of necking in the DN gels determined by uniaxial tensile tests, as shown in **Fig. 3-12a**.

Sample code	1st network			2nd network			Tensile behavior	G_{jump} [J/m^2]	G_{th} [J/m^2]
	AMPS [M]	MBAA [mol%]	α-keto [mol%]	AAm [M]	MBAA [mol%]	α-keto [mol%]			
DN-N1	1	2	1	2.0	0.01	0.01	Necking	–	$\approx 1.35 \times 10^3$
DN-N2	1	4	1	2.0	0.01	0.01	Necking	–	$\approx 2.0 \times 10^3$
DN-U1	1	4	0.1	2.0	0.1	0.1	Unnecking	$\approx 1.0 \times 10^3$	–

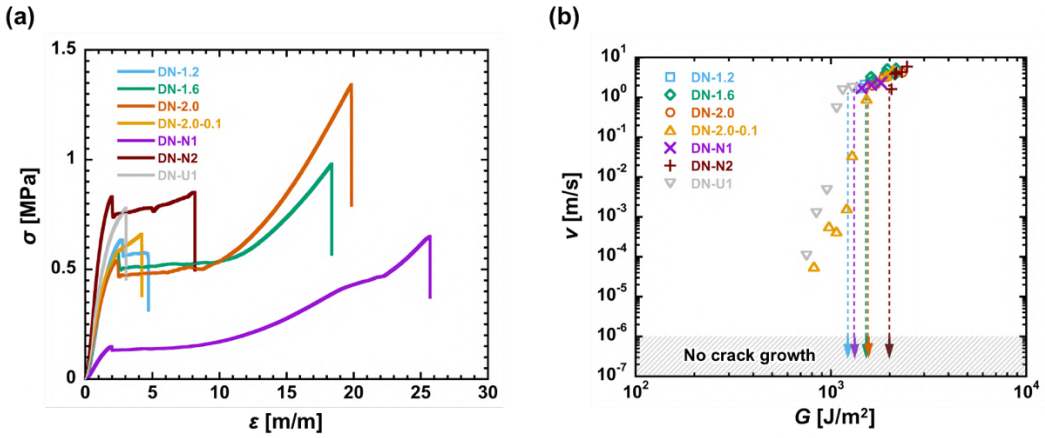

Fig. 3-12. (a) Uniaxial tensile stress–strain curves and (b) logarithmic plots of the energy release rate G and the velocity of crack growth v for all necking and unnecking DN gels with different network compositions. The sample codes are provided in **Table 3-3**. The arrows depict the G at which crack propagation was not detected. The grey hatched regime indicates the crack propagation was not observed within experimental resolution.

3.3.4 Real-time birefringence observation during crack growth

To clarify the reason for the suppression of slow-mode crack propagation by necking DN gels, we examined the optical retardation images around the crack tips of DN gels to identify the necking zones in which the second networks were in highly anisotropic orientations. Previous studies have suggested that, for a necking DN gel, the brittle first network ruptures into clusters above the yielding point with necking [13], and the stretchable second network holds the stress with microscopic elongation along the tensile direction [7]. The degree of molecular orientation of the networks can be determined by retardation R.

Figures 3-13a–c show the optical retardation images for the

representative samples. There was a large difference between the *R* distributions around the crack tips of brittle DN-0.8 with slow-mode crack propagation and the necking DN-2.0 without crack propagation, which suggested the contribution of microscopic molecular conditions to the suppression of slow-mode crack propagation. In the case of brittle DN-0.8, no high *R* area around the crack tip was observed during slow-mode crack propagation. This implied that the sparse second networks were not sufficiently strong to bear the load transferred from the broken first networks; therefore, the two networks broke together at slow speeds. In contrast, in the case of necking DN-2.0, a distinctly strong triangular *R* area was developed around the crack tip at *G* prior to crack propagation. The size of the strong *R* area was on the millimeter scale in both parallel and perpendicular directions to the stretch direction. The maximum *R* at the crack tip (R_{max} = 97.9 nm) was approximately 10 times the average *R* in the bulk (R_{bulk} = 10 nm). This suggested that the dense second network was strong enough to bear the load transferred from the fractured first networks around the crack tips. Moreover, the large strain hardening of the second network further induced fracture of the first network in the crack tip area, which suppressed crack propagation. The large damage zone generated before crack propagation is in agreement with our previous observations [14–16]. This high crack resistance induced by partial stretching of flexible networks from fractured rigid networks is specific to the DN structures consisting of contrasting networks. However, at *G* that the crack propagated in fast mode, *R* becomes very weak. For unnecking DN-2.0-0.1, a slightly high crescent moon-shaped *R* area was noticed at the crack tip (**Fig. 3-13c**), which was substantially smaller than the triangular *R* area of necking DN-

2.0.

Next, we calculated the areas S having higher R than that of the bulk for different G values for necking DN-2.0. Here S was determined as area for R 2 times higher than that of bulk region. The calculated S might not be sufficiently accurate because of variations in manual notching or the resolution limitation of R images. Nevertheless, we observed a decreasing tendency in S with the increase of G near G_{th} (**Fig. 3-13d**). In addition, the R_{max} intensity around the crack tip also decreased once G exceeded G_{th}. These results indicate that the disappearance of the damage zone and the fast-mode crack propagation are intrinsically related. The energy required to form the damage zone sets a high energy barrier for the initiation of crack propagation. Once the energy release rate overcomes the energy barrier to form the damage zone, the crack starts to propagate. As the damage zone size reduces when the crack starts to propagate, the fracture energy decreases while energy release rate keeps constant. Therefore, the excess energy release accelerates the crack propagation, which results in fast mode fracture (brittle fracture).

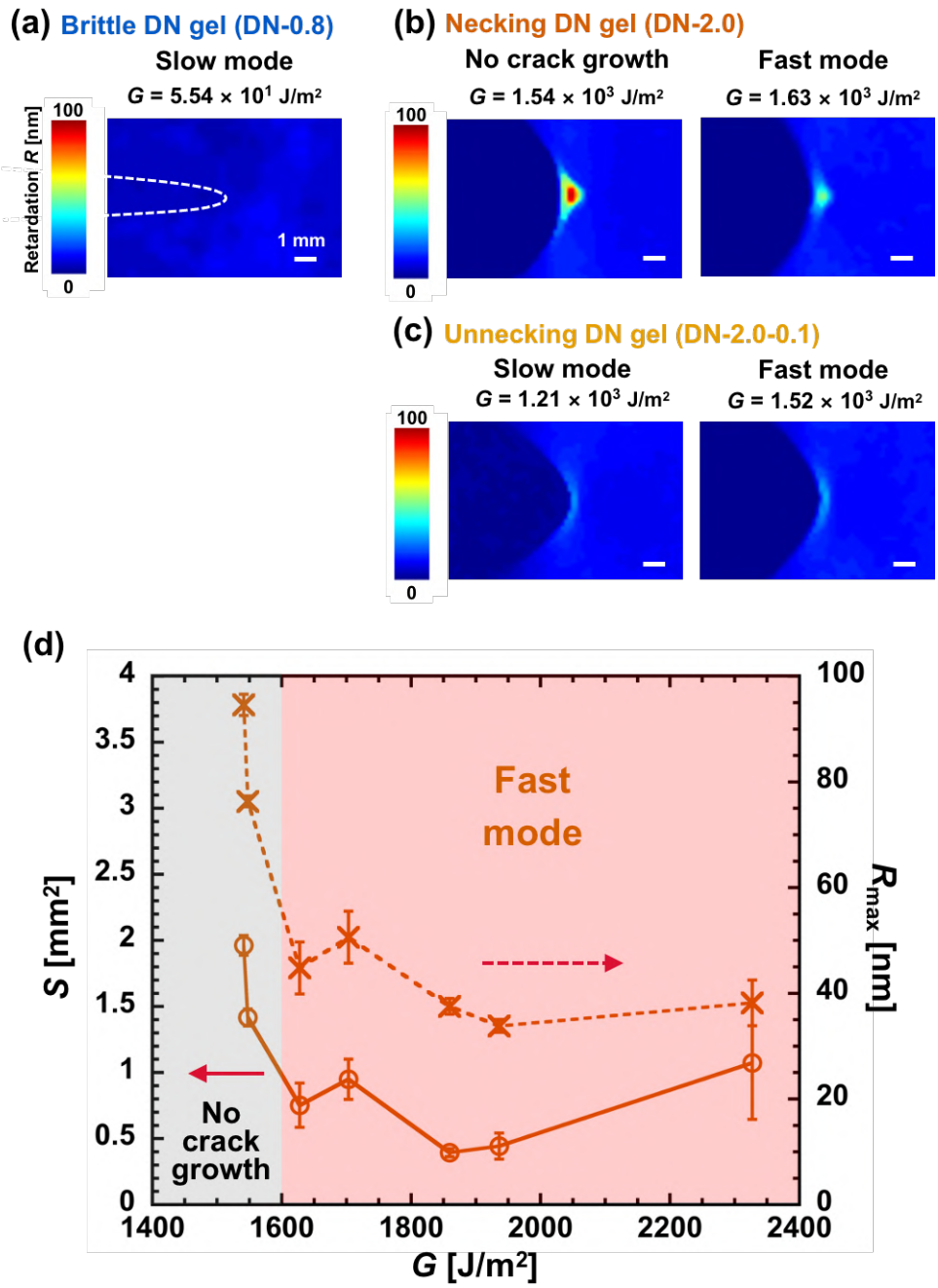

Fig. 3-13. Representative retardation images of (a) DN-0.8, (b) DN-2.0 and (c) DN-2.0-0.1. (d) Corresponding high retardation areas, S, and maximum retardations, R_{max}, at the crack tips of necking DN-2.0 as a function of the energy release rate G. Scale bars represent 1 mm. The white dashed curve in (a) depicts the crack shape of DN-0.8.

3.3.5 Velocity jump

Sakumichi *et al.* and Kubo *et al*. explained the velocity jump of viscoelastic rubbers by a rubber–glass transition around the crack tip with an increase in the strain rate [17,18]. Here we discuss if this explanation is applicable to the slow-to-fast mode transition of hydrogels observed in **Fig. 3-9a** for the SN, brittle and unnecking DN gels. According to the polymer network theory, the dynamics of chemically crosslinked gels is characterized by two relaxation times, the longest Rouse relaxation time τ_R of polymer strands between crosslinking points, and the relaxation time of Kuhn segment τ_0 [19]. Depending on the strain rate ω, crosslinked gels behave elastically at $\omega < \tau_R^{-1}$ with an ω-independent modulus (plateau modulus), viscoelastically at $\tau_R^{-1} < \omega < \tau_0^{-1}$ with a modulus increasing with $\omega^{1/2}$, and glassy like at $\omega > \tau_0^{-1}$ with a high modulus. τ_R depends on the network structure, while τ_0 only depends on Kuhn segment size and is ~10^{-9} s^1 for the synthetic flexible polymers [19]. To discuss the dynamic behavior of the polymer network at the crack tip, we estimate the crack tip strain rate ω_{tip} in the slow mode regime. By rough order estimation, $\omega_{tip} \sim v/r$ where r is the distance from the crack tip [20,21]. The minimum r should be the mesh size ξ for a polymer network, which could be estimated from the Young's modulus using relation $E \approx 3k_BT/\xi^3$, where k_B and T are the Boltzmann' constant and absolute temperature, respectively [19,22]. For SN-2.0, $\tau_R \sim 10^{-4}$ s^1, which is obtained from a PAAm hydrogel with a comparable modulus [23]. On the other hand, the strain rate experienced by the polymer network near the crack tip was $\omega_{tip} \sim 10^4$–10^5 s^{-1} for $v \sim 10^{-4}$–10^{-3} m/s using $\xi \sim 8.8$ nm ($E = 18.1$ kPa, **Table 3-2**). Accordingly, at the crack tip, $\omega_{tip}\tau_R \sim 1$–10, and the network responses viscoelastically. This explains

the v-dependence of $\Gamma(v)$ even in the slow mode regime. However, since $\omega_{tip}\tau_0 \sim 10^{-4} << 1$ even for the maximum velocity before the velocity jump ($\sim 10^{-3}$ m/s), the slow-to-fast mode transition could not be explained by the rubber-glass transition around the crack tip for the SN gel. We consider that when G increased to the G_{jump}, $G = \Gamma$ is no longer hold, and the excess energy release rate, $G - \Gamma > 0$, might accelerates the crack propagation to fast mode. Later, the accelerated crack is affected by inertia effect, which results in the steady-state v at fast mode [6]. Consequently, we observed a sudden velocity jump at G_{jump}. The same explanation could be applied to the velocity jump of brittle DN gel and unnecking DN gel, which show the maximum velocity before the velocity jump of $\sim 10^{-3}$–10^{-2} m/s.

3.3.6 Suppression of slow mode in necking DN gels

The results of crack growth tests and birefringence observations suggest that the existence of a large damage zone around the crack tip plays an important role in the suppression of slow-mode crack propagation. To understand why the slow-mode crack propagation is suppressed for the necking DN gels, we discussed the energy balances of the necking DN gels during crack initiation. As reported in previous studies [10,24], the fracture energy at crack initiation Γ_c can be described as follows:

$$\Gamma_c = \Gamma_0 + \Gamma_{dis} \approx \Gamma_0 + U_{dis}h \qquad (3.3)$$

where Γ_0 is the intrinsic Γ of the damage zone, Γ_{dis} is the dissipated energy because of the formation of the damage zone, U_{dis} is the mechanical hysteresis density, and

h is the characteristic size of the damage zone defined in the undeformed state in the stretching direction. When G approaches Γ_c, damage zones with long h around the crack tips develop in the necking DN gels, which results in an extraordinarily high Γ_c.

Theoretical and experimental results indicate that near the crack tip, uniaxial tension dominates for a highly deformable soft solid under mode-I plane-stress conditions [25,26]. Using this uniaxial approximation, we can roughly consider that U_{dis} is equal to the work of extension to fracture W_f of the unnotched sample under uniaxial tension, namely, $U_{dis} \approx W_f$. If we suppose that $\Gamma_{dis} >> \Gamma_0$ at the onset of crack initiation ($G = G_{th} \approx \Gamma_c$), equation (4) can be presented as

$$G_{th} \approx W_f h \qquad (3.4)$$

, which provides

$$h \approx G_{th} / W_f \qquad (3.5)$$

In the case of DN-2.0, h was estimated to be ≈ 132 μm from equation (3.5) using $W_f \approx 12.1$ MJ/m^3 and $G_{th} \approx 1.6 \times 10^3$ J/m^2 obtained by uniaxial tensile tests and crack growth tests. Because h is the undeformed size of the damage zone, h multiplied by the fracture stretch ratio λ_f (≈ 18.0) affords the damage zone in the deformed state, which was estimated as $h\lambda_f \approx 2.4$ mm. This value is almost identical to the height of the high R area at $G \leq G_{th}$ acquired by the R images, that is, ~ 2.76 mm (**Fig. 3-13b**). This justifies again that the high Γ_c of the necking DN gels is due to their large damage zones, as described in equation (3.3).

Subsequently, we discussed the energy balance after crack initiation. Once G reaches G_{th} and the crack starts to propagate, the damage zone cannot

develop for the necking DN samples, as indicated by the reduction of S and R_{max} in **Fig. 3-13d**. Therefore, Γ_{dis} decreases, and Γ becomes less than that at crack initiation, namely, $\Gamma < \Gamma_c$. The excessive energy release $G - \Gamma > 0$ at onset of crack propagation leads to crack acceleration. This explains why the necking DN gels show only fast-mode crack propagation.

Then, the final question is why the damage zone disappears at $G > G_{th}$ after crack initiation? We consider that this phenomenon is also related to the dynamics of the polymer network. The damage zone develops via continuous internal deformation and load transfer process, including loading and breakage of the first network, transfer of load to the second network, deformation and strain hardening of the second network to induce further breakage of the first network. Such process should repeat until the tension on the surface of the crack becomes high enough to activate the breakage of second network strands on the surface, and the larger the damage zone, the longer the time required for this process. Therefore, for the necking DN gels, once the crack starts to propagate even at in slow speed, the strain rate at the crack tip is already high in viscoelastic regime ($\omega_{tip}\tau_R > 1$), therefore, there is insufficient time for the formation of a damage zone far from the crack tip. Our recent study on the crack initiation of pre-notched necking DN gels also suggests a strong influence of the second network dynamics on the size of damage zone [27].

3.3.7 Crack growth behavior of DN gels with denser second network

We further studied on the crack propagation behaviors of DN gels prepared with the denser second network composition (C_2 = 4.0 and 8.0 M). **Fig.**

3-14a shows the uniaxial tensile behaviors of DN gels prepared with the high second network concentrations. DN-4.0 showed the yielding of stress, but the abrupt decrease of the stress and the necking phenomenon did not occur like DN-2.0. Furthermore, when C_2 increased to 8.0 M, the sample lost the high stretchability, and a slight decrease of the slope of stress–strain curve was observed. As shown in **Fig. 3-14b** and **3-14c**, the gap of the $(n+1)^{th}$ loading and the n^{th} unloading curves during cyclic tensile tests became bigger with the increase of C_2, which indicates that the tensile behaviors of the DN gels with much dense second networks exhibit viscoelasticity.

Figure 3-15 depicts the power-law relationship between G and v for their samples where G was calculated from the regression curves of $W_{\mathrm{unloading},n}(\varepsilon_{\mathrm{max},n})$ (**Fig. 3-14d**). DN-4.0 showed only fast mode and high G_{th} of ~ 1.65×10^3 J/m^2, which indicates that this sample also can suppress the slow mode (**Table 3-4**). On the other hand, DN-8.0 showed much lower G_{th} of ~ 5.0×10^2 J/m^2 than that of other DN gels showing the suppression of the slow mode, and its v easily reached its shear wave speed above G_{th}. Although the tensile behavior of DN-8.0 were similar with DN-2.0-0.1 that showed the slight yielding of the stress and the unnecking behavior, the slow-mode crack propagation could not be observed.

The retardation images of these samples were significantly different from the necking samples, and the butterfly-like retardation patterns were formed around the crack tips (**Fig. 3-16**). Since such birefringence patterns were often reported in viscoelastic gels [28], the complicated viscoelasticity derived from a large amount of entanglement points of the second network dominates the stress or strain fields of the DN gels with the dense second networks, which results in a

collapse of the strong correlation between the tensile behaviors and the crack propagation behaviors which are confirmed in the DN gels with relatively low second network concentrations.

Table 3-4. A list of parameters related to crack propagation in the fast mode for the DN gels with high second network concentrations.

Sample code	E [MPa]	c_s [m/s]	G_{th} [J/m^2]
DN-4.0	0.245 ± 0.006	9.0	≈ 1.65 × 10^3
DN-8.0	0.241 ± 0.005	9.0	≈ 5.0 × 102

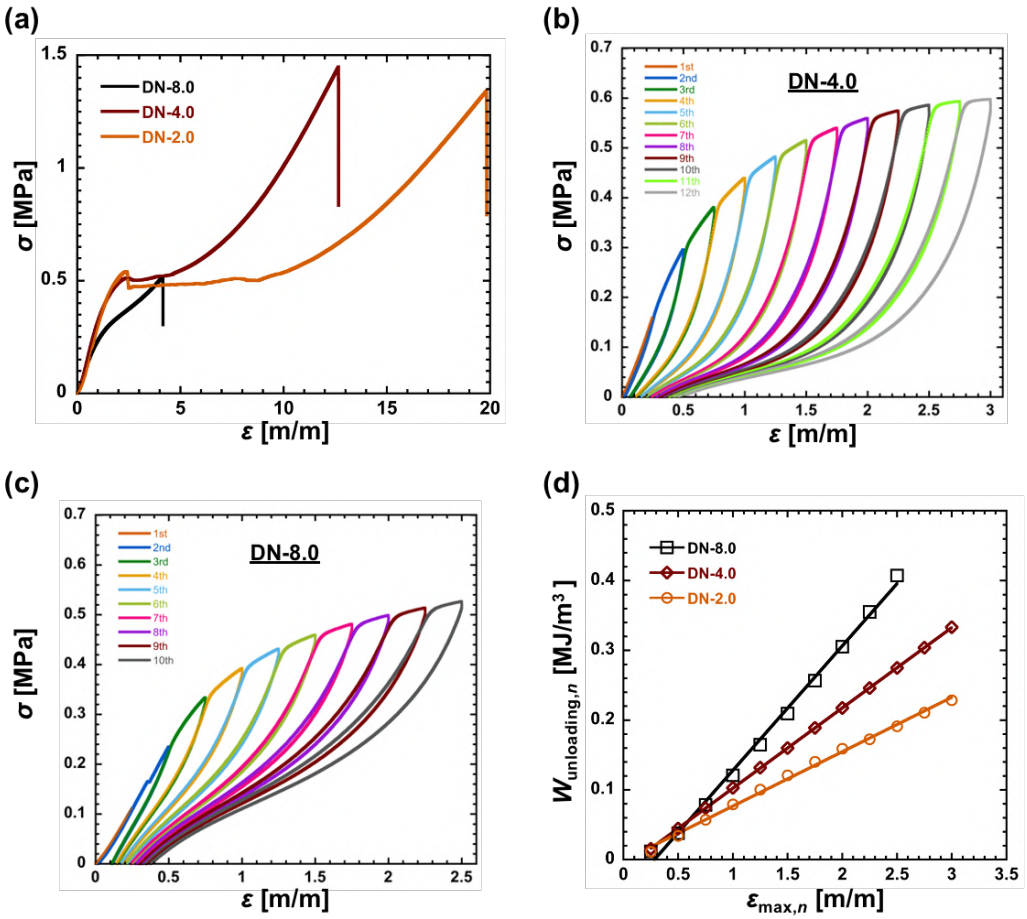

Fig. 3-14. (a) Uniaxial tensile stress–strain curves of the DN gels with high second network concentrations. Cyclic tensile stress–strain curves of the unnotched samples measured in pure shear geometries of (b) DN-4.0 and (c) DN-8.0. (d) Dependence of $W_{\text{unloading}}$ on $\varepsilon_{\text{max},n}$ of the DN gels with high second network concentrations. For (a) and (d), the data of necking DN-2.0 are also shown for comparison.

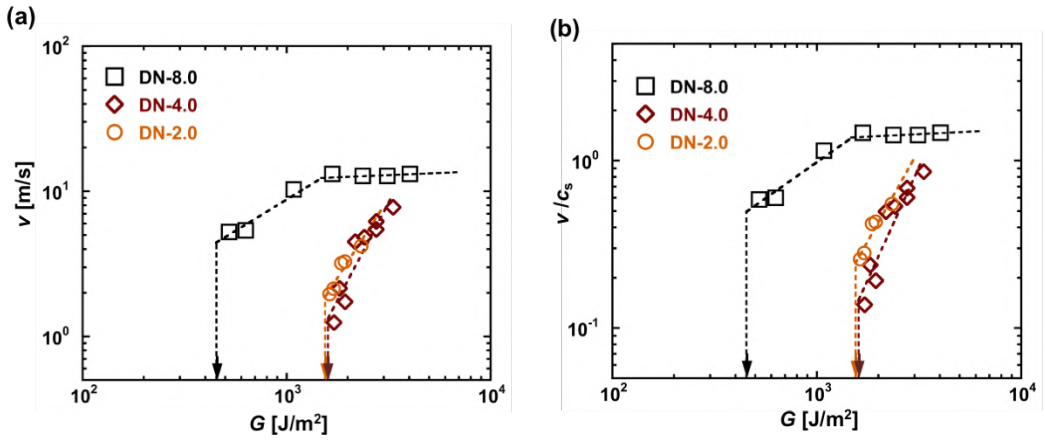

Fig. 3-15. (a) Logarithmic plots of the energy release rate G and the velocity of crack growth v for the DN gels with high second network concentrations. The arrows depict the G at which crack propagation was not detected. (c) Logarithmic plots of G and v normalized by the shear wave speed c_s. The data of necking DN-2.0 are also shown for comparison.

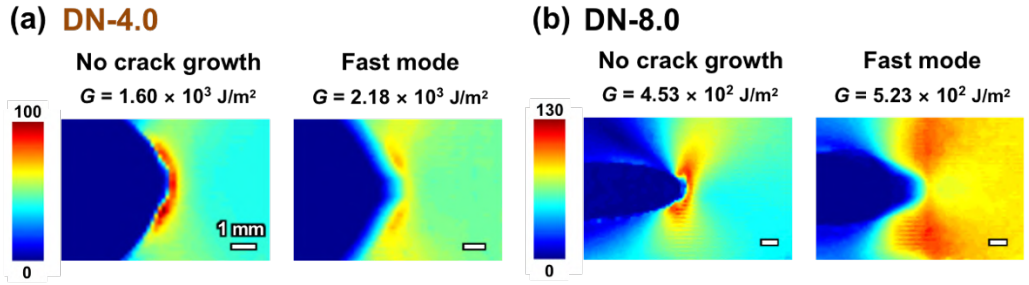

Fig. 3-16. Representative retardation images of (a) DN-4.0 and (b) DN-8.0.

3.4 Conclusions

Crack propagation of DN hydrogels under various tensions was systematically studied for the first time. Strong correlations between the crack growth behaviors of the DN gels under tension and their uniaxial tensile behaviors were observed. The crack growth velocity v of the brittle or unnecking DN gels exhibited slow mode at relatively low strain energy release rate G and it jumped to the fast mode above a critical G_{jump}, in similar to SN gels and rubbery materials reported. In contrast, for the necking DN gels, the crack propagation was initiated at a very high threshold G_{th}, above which the crack propagated at fast mode, without via the slow mode. We found that the large threshold G_{th} and the suppression of the slow-mode crack propagation in the necking DN gels were related to the creation of damage zone around the crack tip. A large damage zone was formed at G slightly smaller than G_{th}, prior to the crack propagation, while the damage zone almost vanished once the crack started to propagate above G_{th}. The damage zone formation, which consumes large amount of energy due to breaking of the brittle sacrificial network, sets a high energy barrier for crack initiation; once the crack starts to propagate, the crack propagation is too fast to allow the full development of damage zone. As a result, the elastic energy released by the overstretched DN gels surpasses the fracture energy for crack advancing, and the crack is accelerated to reach the fast mode. Accordingly, we consider that the unique behavior of necking DN gels is attributed to insufficient time for damage zone formation at the crack tip. The large G_{th} demonstrates the excellent crack initiation resistance Γ_c (= G_{th}) of necking DN gels under high tension. We believe that the unique crack resistance characterized in this work is important for

practical design of DN gels as load-bearing materials.

3.5 Reference

[1] Y. Zhang, K. Fukao, T. Matsuda, T. Nakajima, K. Tsunoda, T. Kurokawa, J. P. Gong, Unique Crack Propagation of Double Network Hydrogels under High Stretch, *Extrem. Mech. Lett.*, 51 (2022) 101588.

[2] S. Ahmed, T. Nakajima, T. Kurokawa, M. Anamul Haque, J. P. Gong, Brittle-Ductile Transition of Double Network Hydrogels: Mechanical Balance of Two Networks as the Key Factor, *Polymer*, 55 (2014) 914–923.

[3] R. S. Rivlin, A. G. Thomas, Rupture of Rubber. I. Characteristic Energy for Tearing, *J. Polym. Sci.*, 10 (1953) 291–318.

[4] R. Long, C.-Y. Hui, Fracture Toughness of Hydrogels: Measurement and Interpretation, *Soft Matter*, 12 (2016) 8069–8086.

[5] T. Onuma, Y. Otani, A Development of Two-Dimensional Birefringence Distribution Measurement System with a Sampling Rate of 1.3 MHz, *Opt. Commun.*, 315 (2014) 69–73.

[6] T. Goldman, A. Livne, J. Fineberg, Acquisition of Inertia by a Moving Crack, *Phys. Rev. Lett.*, 104 (2010) 5–8.

[7] T. Nakajima, T. Kurokawa, S. Ahmed, W. Wu, J. P. Gong, Characterization of Internal Fracture Process of Double Network Hydrogels under Uniaxial Elongation, *Soft Matter*, 9 (2013) 1955–1966.

[8] K. Fukao, T. Nakajima, T. Nonoyama, T. Kurokawa, T. Kawai, J. P. Gong, Effect of Relative Strength of Two Networks on the Internal

Fracture Process of Double Network Hydrogels As Revealed by *in Situ* Small-Angle X-Ray Scattering, *Macromolecules*, 53 (2020) 1154–1163.

[9] T. Matsuda, T. Nakajima, Y. Fukuda, W. Hong, T. Sakai, T. Kurokawa, U. Il Chung, J. P. Gong, Yielding Criteria of Double Network Hydrogels, *Macromolecules*, 49 (2016) 1865–1872.

[10] T. Nakajima, T. Kurokawa, H. Furukawa, J. P. Gong, Effect of the Constituent Networks of Double-Network Gels on Their Mechanical Properties and Energy Dissipation Process, *Soft Matter*, 16 (2020) 8618–8627.

[11] K. Tsunoda, J. J. C. Busfield, C. K. L. Davies, A. G. Thomas, Effect of Materials Variables on the Tear Behaviour of a Non-Crystallizing Elastomer, *J. Mater. Sci.*, 35 (2000) 5187–5198.

[12] Y. Morishita, K. Tsunoda, K. Urayama, Velocity Transition in the Crack Growth Dynamics of Filled Elastomers: Contributions of Nonlinear Viscoelasticity, *Phys. Rev. E*, 93 (2016) 1–11.

[13] J. P. Gong, Why Are Double Network Hydrogels so Tough?, *Soft Matter*, 6 (2010) 2583–2590.

[14] Q. M. Yu, Y. Tanaka, H. Furukawa, T. Kurokawa, J. P. Gong, Direct Observation of Damage Zone around Crack Tips in Double-Network Gels, *Macromolecules*, 42 (2009) 3852–3855.

[15] S. Liang, Z. L. Wu, J. Hu, T. Kurokawa, Q. M. Yu, J. P. Gong, Direct Observation on the Surface Fracture of Ultrathin Film Double-Network Hydrogels, *Macromolecules*, 44 (2011) 3016–3020.

[16] T. Matsuda, R. Kawakami, T. Nakajima, J. P. Gong, Crack Tip Field of a

Double-Network Gel: Visualizing Covalent Bond Scission by Mechanoradical Polymerization, *Macromolecules*, 53 (2020) 8787–8795.

[17] N. Sakumichi, K. Okumura, Exactly Solvable Model for a Velocity Jump Observed in Crack Propagation in Viscoelastic Sheets, *Sci. Rep.*, 7 (2016) 1–11.

[18] A. Kubo, N. Sakumichi, Y. Morishita, K. Okumura, K. Tsunoda, K. Urayama, Y. Umeno, Dynamic Glass Transition Dramatically Accelerates Crack Propagation in Rubberlike Solids, *Phys. Rev. Mater.*, 5 (2021) 1–14.

[19] M. Rubinstein, R. H. Colby, *Polymer Physics*; Oxford University Press, (2003).

[20] P. G. De Gennes, Soft Adhesives, *Langmuir*, 12 (1996) 4497–4500.

[21] B. N. J. Persson, O. Albohr, G. Heinrich, H. Ueba, Crack Propagation in Rubber-like Materials, *J. Phys. Condens. Matter*, 17 (2005) 1071–1142.

[22] H. Guo, Y. Uehara, T. Matsuda, R. Kiyama, L. Li, J. Ahmed, Y. Katsuyama, T. Nonoyama, T. Kurokawa, Surface Charge Dominated Protein Absorption on Hydrogels, *Soft Matter*, 16 (2020) 1897–1907.

[23] B. A. Krajina, C. Tropini, A. Zhu, P. Digiacomo, J. L. Sonnenburg, S. C. Heilshorn, A. J. Spakowitz, Dynamic Light Scattering Microrheology Reveals Multiscale Viscoelasticity of Polymer Gels and Precious Biological Materials, *ACS Cent. Sci.*, 3 (2017) 1294–1303.

[24] Y. Tanaka, A Local Damage Model for Anomalous High Toughness of Double-Network Gels, *Europhys. Lett.*, 78 (2007) 56005.

[25] R. Long, C. Y. Hui, Crack Tip Fields in Soft Elastic Solids Subjected to

Large Quasi-Static Deformation - A Review, *Extrem. Mech. Lett.*, 4 (2015) 131–155.

[26] Y. Qi, Z. Zou, J. Xiao, R. Long, Mapping the Nonlinear Crack Tip Deformation Field in Soft Elastomer with a Particle Tracking Method, *J. Mech. Phys. Solids*, 125 (2019) 326–346.

[27] Y. Zheng, T. Matsuda, T. Nakajima, W. Cui, Y. Zhang, C.-Y. Hui, T. Kurokawa, J. P. Gong, How Chain Dynamics Affects Crack Initiation in Double-Network Gels, *Proc. Natl. Acad. Sci.*, 118 (2021) e2111880118.

[28] F. Luo, T. L. Sun, T. Nakajima, T. Kurokawa, Y. Zhao, A. Bin Ihsan, H. L. Guo, X. F. Li, J. P. Gong, Crack Blunting and Advancing Behaviors of Tough and Self-Healing Polyampholyte Hydrogel, *Macromolecules*, 47 (2014) 6037–6046.

Chapter 4: Crack Shapes of DN gels

4.1 Introduction

As reported in **Chapter 3**, the great crack resistances and the unique crack propagation behaviors of DN gels were demonstrated. In **Chapter 4**, we further studied on the crack shapes of DN gels during propagation. In previous works on the crack shapes of soft materials, the local fracture mechanism around crack tips has been discussed by capturing shapes of cracks [1–6]. For elastic materials, crack should become a parabolic shape, which is predicted by linear elastic fracture mechanics (LEFM) [7,8]. However, for brittle fracture, a deviation from a parabolic shape is observed in the vicinity of cracks that propagate at very fast speed. Livne *et al*. demonstrated it by using PAAm gels [1], and Morishita *et al*. found that it also appears in rubber materials [4], both of which indicate the existence of a strongly nonlinear zone around crack tip. For DN gels, Kolvin *et al*. demonstrated that the crack shapes of DN gels are unique and much differ from other materials above mentioned [9]. In addition, crack tip opening displacement (CTOD) $2\delta_c$, which is defined as the displacement between two points where crack contours are intersected by two symmetric rays originating from the crack tip with a 90° angle at crack initiation, is a widely used as a crack shape parameter to evaluate crack resistances of practical materials [10–13]. For soft materials, half CTOD δ_c is often related with the nonlinear elastic scale G/E where G is energy release rate and E is Young's modulus, which is derived from LEFM and corresponds to the length scale where nonlinearity dominates the fracture behaviors. Scaling analysis indicates that $\delta_c \sim G/E$ is confirmed [5,14], and a recent work by Zheng *et al*. revealed that it is also preserved in the crack initiation of DN

gels [6].

The purpose of this study is revealing the relationship between polymer network structure and crack shape of DN gels and elucidating the crack propagation mechanism. We captured the crack shapes of DN gels prepared with different compositions from the images taken by the crack growth tests performed in **Chapter 3** [15]. We analyzed them and described these profiles by fitting them with $x = (x_0 +) ay^b$. From the fitting parameters a and b, we calculated the CTOD length scale ℓ and compared them with the nonlinear elastic scale G/E. Finally, we evaluated the energy flux around crack tip by analogic scaling with LEFM and discussed how it contributes to the fracture mechanism of the DN gels.

4.2 Experiments

4.2.1 Material & synthesis of DN gels

PAMPS/PAAm DN gels prepared in **Chapter 3** were used (see section ***3.2.1*** and ***3.2.2***) [15]. The polymer structures of these samples were varied by changing the first network cross-linker density x_1, the second network concentration C_2 and the second network cross-linker density x_2, which are the in-feed concentrations used in each precursor solution (reshown in **Table 4-1**). In this study, for simplicity, DN gels were denoted as DN(x_1/C_2(-x_2)). Unless otherwise stated, x_2 was 0.01 mol%.

Table 4-1. A list of formulations and properties of the samples used in this study.

Composition	AMPS [M]	AAm C_2 [M]	MBAA x_1, x_2 [mol%]	α-keto [mol%]
1st network	1	−	2, 3, 4	0.01
2nd network	−	1.2, 2.0, 4.0	0.01, 0.1	0.01

All the concentrations mentioned are the in-feed concentrations used in the precursor solutions.

4.2.2 Mechanical properties of DN gels

We used the data of the mechanical parameters of each DN gel obtained in **Chapter 3**, such as the stress–strain curves and the Young's moduli obtained by the uniaxial tensile tests, those obtained by the cyclic tensile test in pure shear geometries, energy release rates (see section ***3.2.3***, ***3.2.4,*** and ***3.2.5***) [15]. For DN(2/2.0) and DN(4/2.0), whose cyclic tensile stress–strain curves are not shown in **Chapter 3**, those obtained by the cyclic tensile tests of the unnotched samples in pure shear geometries are shown in **Fig. 4-1a** and **Fig. 4-1b**. For DN(3/2.0-0.1), since the cyclic tensile stress–strain curves are displayed only in the region of $\varepsilon \leq 2.5$ where the crack growth tests were conducted in **Chapter 3**, the cyclic stress–strain curves extended to the region of $\varepsilon \leq 3.0$ is also shown in **Fig. 4-1c**.

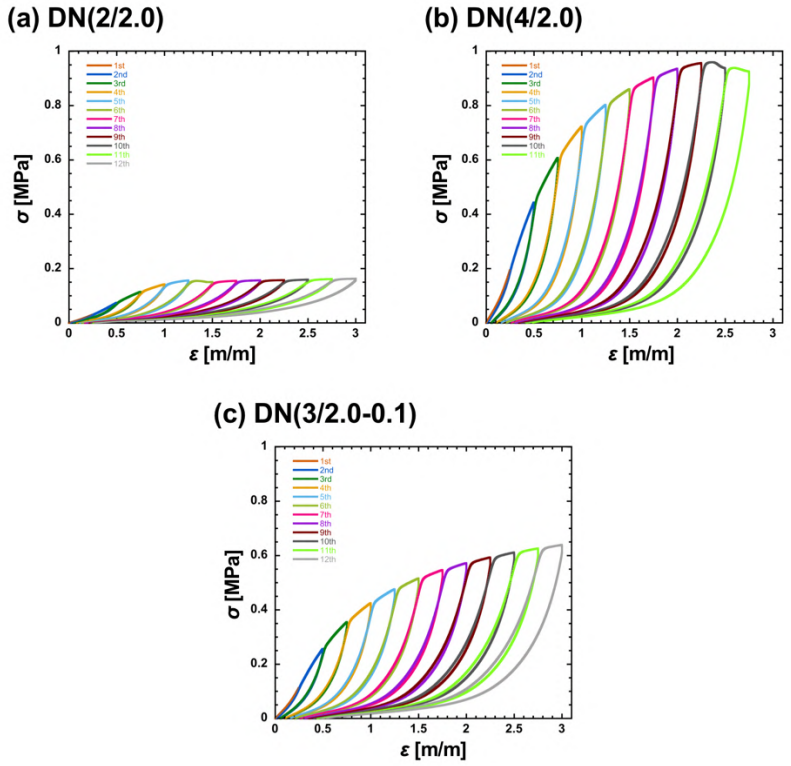

Fig. 4-1. Cyclic tensile stress–strain curves of the unnotched samples measured in pure shear geometries of (a) DN(2/2.0), (b) DN(4/2.0) and (c) DN(3/2.0-0.1).

4.2.3 Image analysis of crack shapes

Crack shapes of DN gels were captured from the images obtained by the crack growth test for the post-notched cracks in **Chapter 3**. As shown in **Fig. 4-2**, the contours of the crack shapes were extracted within $|y| \leq 6$ mm, then, the crack curves were binarized by using ImageJ software. Next, the curves were fitted by an equation of $x = x_0 + ay^b$ where x and y are perpendicular and parallel direction to the stretch axis. The origins of axes were set at the crack tips. It should be noted that it was difficult to determine the crack tips exactly for the crack propagation in high speed because the contrasts of the images were weak due to the transparent condition of the samples for the birefringence measurements and because the resolution of ~ 80 μm and the frame rate of 3000 fps were relatively lower than

the previous work (the resolution of 20 μm and the frame rate of 8000 fps in [9]). Therefore, in this study, we newly set the intercept term x_0 in addition to $x = ay^b$, which enables the accurate evaluation of the parameters a and b. The crack propagations in too high v (> 6 m/s) were excluded in this study in order to capture the crack contours accurately. By analyzing the crack shapes for 3–5 frames, the averaged a and b were calculated for each crack propagation. From these results, the half CTOD length scale ℓ provided in the previous work [9] was calculated as

$$\ell = a^{-1/(b-1)} \qquad (4.1).$$

Since combining $x = ay^b$ and $x = y$ (CTOD) gives $x = y = a^{-1/(b-1)} = \ell$, ℓ corresponds to the half CTOD length. Especially, when the crack was highly broadened or located near the sample edges, the CTOD could not be obtained because the symmetric rays originating from the crack tip with a 90° angle did not intersect the crack contour. However, the equation (4.1) enables to calculate the CTOD in such situation.

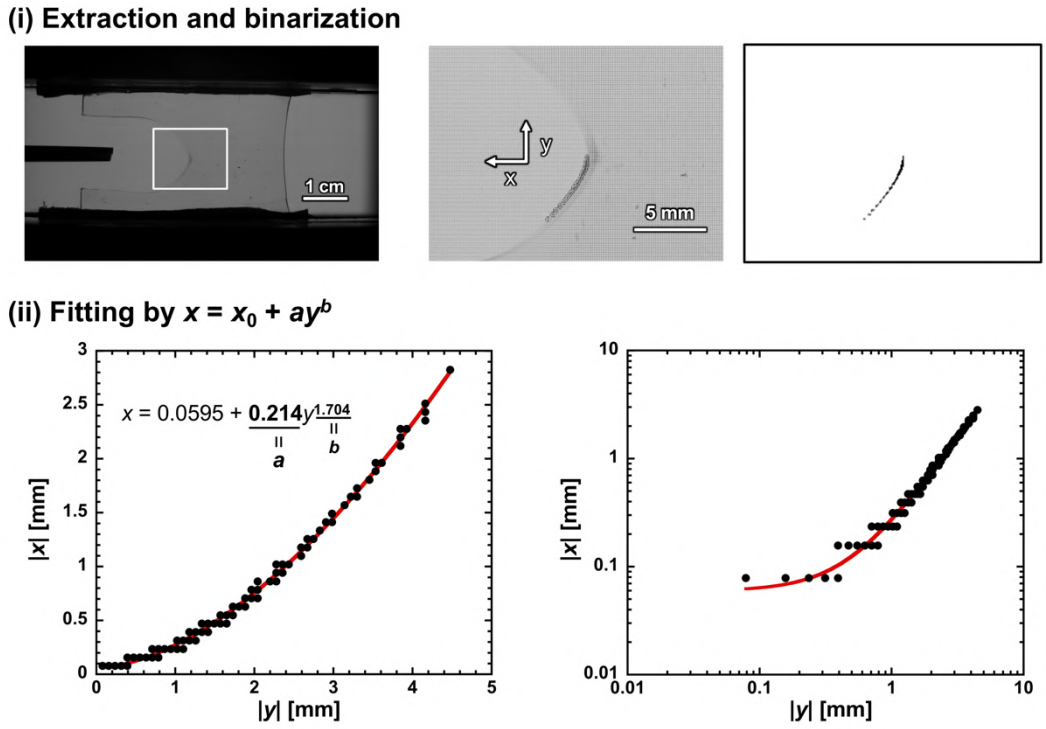

Fig. 4-2. Procedure of crack shape analysis. (i) The contour was extracted and binarized by imageJ software. (ii) The extracted curve was fitted by $x = x_0 + ay^b$.

4.3 Results & discussions

4.3.1 Characterization of crack shapes

Figures 4-3 and **4-4** depict the parameters of the crack shapes of DN gels. Although the a at G much higher than G_{th} was not lower than that of G around G_{th} for DN(3/2.0) and DN(3/4.0), a decreased with increase of G and v in almost samples, which agree with previous work [9]. Besides the data where the crack did not propagate ($G < G_{th}$), the averaged b over all crack propagation, b_{ave}, were in the range of 1.5–1.8 as shown in **Table 4-2**, and all samples showed the crack blunting during crack propagation which is different from a parabolic shape (b = 2) predicted by LEFM. DN(4/2.0), which was prepared in the same formulation as the poly(2-acrylamido-2-methylpropane sulfonic acid sodium

salt)(PNaAMPS)/PAAm DN gels used in previous study [9], showed b_{ave} of 1.60 ± 0.06, which was comparable with the previous one of 1.64 ± 0.08. The higher G (and v), the longer ℓ for all samples, which also show good agreement with the previous work.

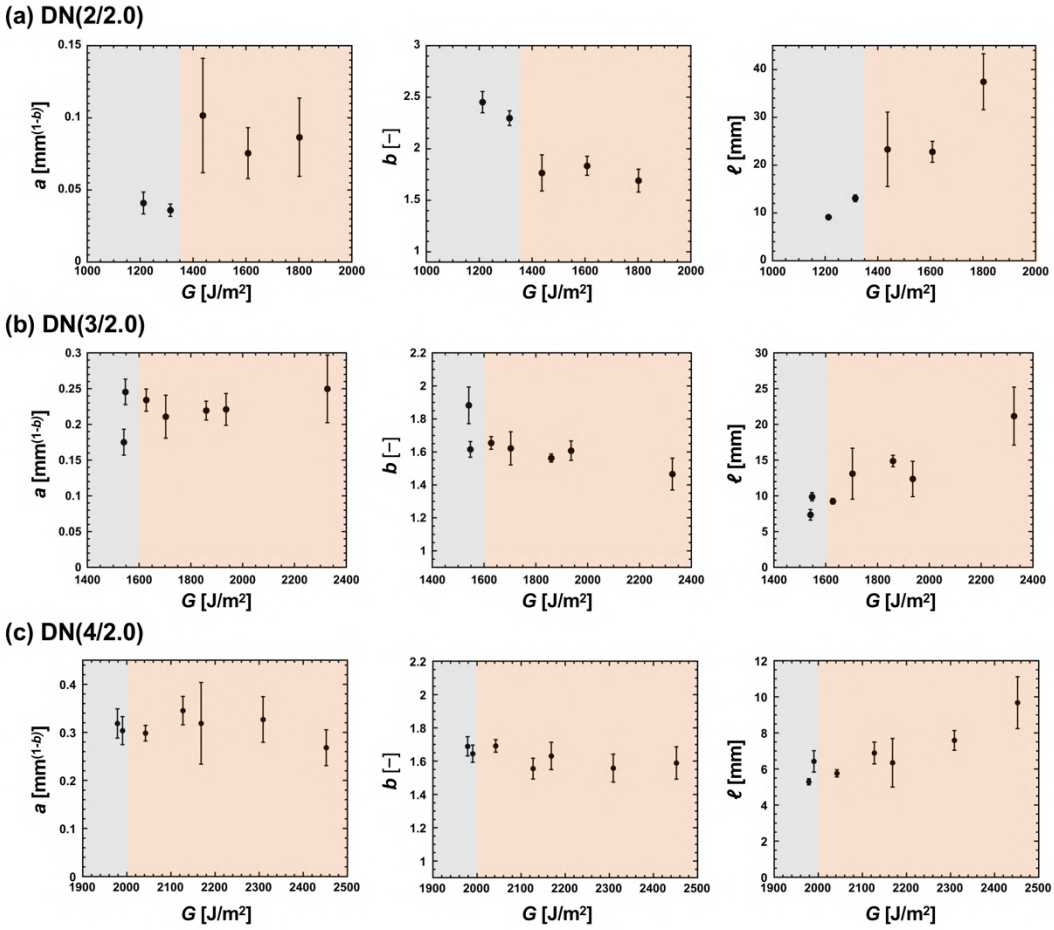

Fig. 4-3. Crack shape parameters a, b, and half CTOD length scale ℓ of the DN gels with the different first network compositions. Black area indicates the crack did not propagate at $G < G_{th}$, and red area indicates the crack propagated in fast mode at $G > G_{th}$.

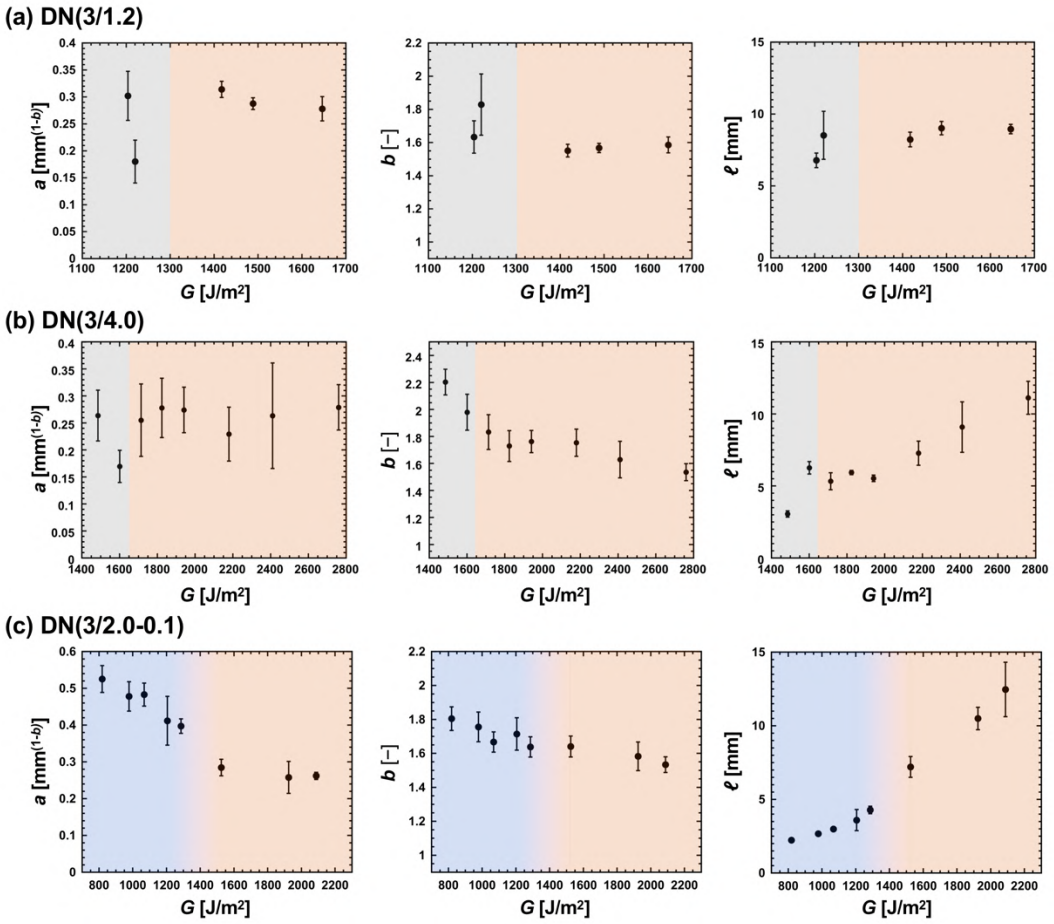

Fig. 4-4. Crack shape parameters a, b, and half CTOD length scale ℓ of the DN gels with the different second network compositions. Black area indicates the crack did not propagate at $G < G_{th}$, red area indicates the crack propagated in fast mode at $G > G_{th}$ or $G > G_{jump}$, and blue area indicated the crack propagated in slow mode at $G < G_{jump}$.

Table 4-2. A list of the parameters related with crack shape parameter b. b_{ave} is the averaged b over all crack propagations, and E is the Young's modulus obtained by uniaxial tensile tests in **Chapter 3** [15].

Sample code		b_{ave} [−]	E [MPa]
DN(2/2.0)		1.76 ± 0.07	0.049 ± 0.003
DN(3/2.0)		1.58 ± 0.07	0.174 ± 0.005
DN(4/2.0)		1.60 ± 0.06	0.266 ± 0.017
DN(3/1.2)		1.57 ± 0.02	0.136 ± 0.013
DN(3/4.0)		1.71 ± 0.11	0.245 ± 0.006
DN(3/2.0-0.1)	Slow mode	1.74 ±0.06	0.187 ± 0.008
	Fast mode	1.60 ±0.05	

b_{ave} of each sample varied, and DN(2/2.0) showed relatively high b. Kolvin *et al*. predicted that this lower b than 2 observed in DN gel is derived from the strain-stiffening behavior after damaged by pre-loading [9,16]. To demonstrate it, we investigated the relationship between b and the stiffness properties of the DN samples.

Fig. 4-5 shows the relationship between the Young's moduli obtained by uniaxial tensile tests and the b_{ave} only for the fast-mode crack propagations, but there is no clear correlation. Next, the unloading curves obtained by the cyclic tensile tests were compared, which commonly shows steep increases of the stress near the maximum strain of loading ε_{max} [16–18]. As shown in **Fig. 4-6**, the unloading curves normalized by the maximum stress and the maximum strain of each cycle were collapsed on master curves after yielding for the DN gels that

showed yielding during the cyclic tensile tests (DN(2/2.0), DN(3/2.0) and DN(4/2.0)), and the curves hardly differed at $\varepsilon_{max} \geq 2.25$ for the DN gels that did not show yielding during the cyclic tensile tests (DN(3/1.2), DN(3/4.0) and DN(3/2.0-0.1)). Therefore, each normalized unloading curve at $\varepsilon_{max} = 2.5$ were compared as shown in **Fig. 4-7**. The gentlest curve was that of DN(2/2.0), the second was that of DN(3/4.0), and the other's curves were almost the same. This order correlates with the order of the magnitude of b_{ave}, which implies that the abrupt strain-hardening of the pre-damaged states might contributes to the nonparabolicity of crack shapes of DN gels. In other words, the contrast between the mechanical strengths of both individual networks is assumed to affect the crack shapes of DN samples since the strength of the first network is relatively weak in DN(2/2.0) and the strength of the second network is relatively strong in DN(3/4.0) [19].

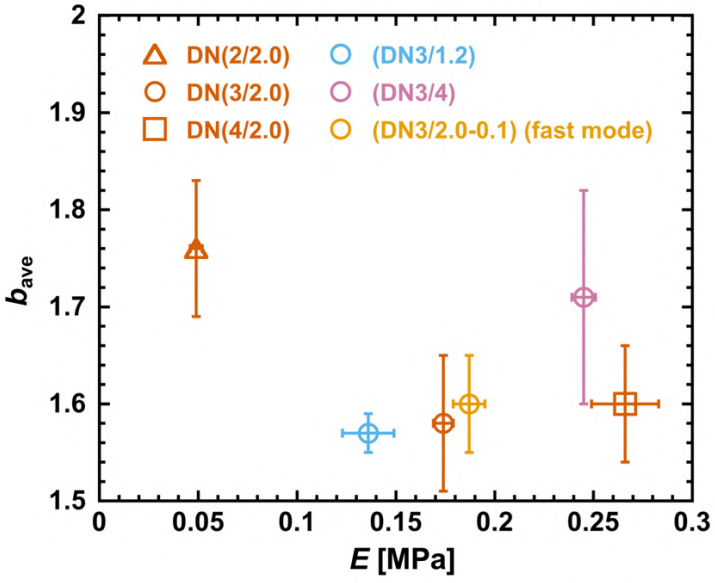

Fig. 4-5. Relationship between the Young's moduli and b_{ave} for fast-mode crack propagations of each sample.

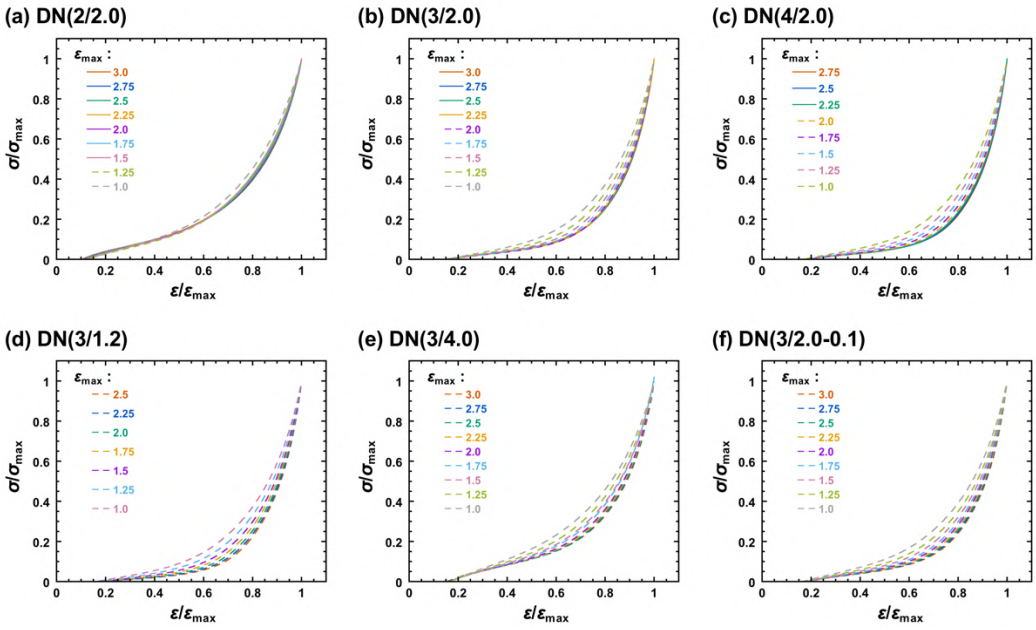

Fig. 4-6. Unloading stress–strain curves obtained by the cyclic uniaxial tensile test of the DN samples in pure shear geometries in **Chapter 3** [15] normalized by the maximum stress σ_{max} and the maximum strain ε_{max} of each cycle. The curves in solid line indicate that the bulk samples already reached the yielding points during pre-loading, and the curves in dashed line indicate the bulk samples did not show the yielding points during pre-loading.

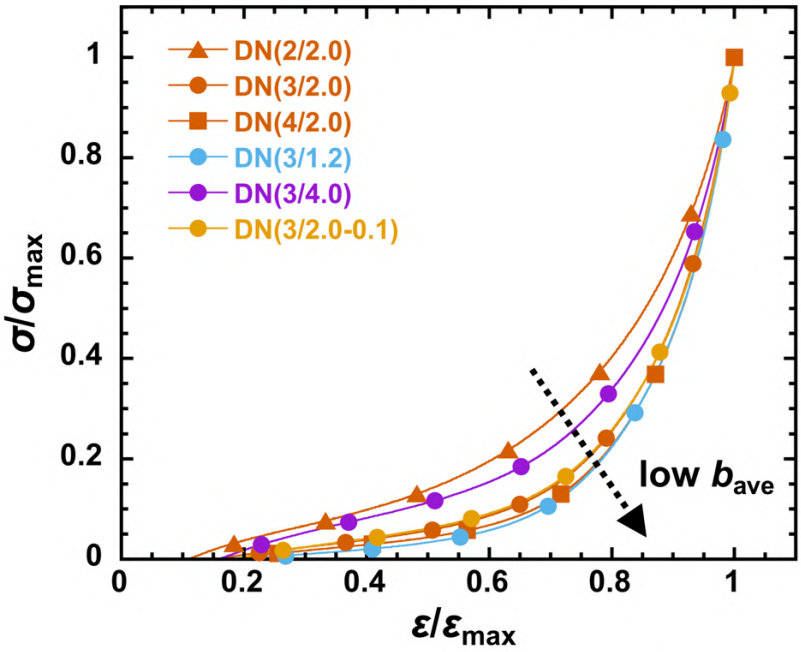

Fig. 4-7. Unloading stress–strain curves of each sample after pre-loaded at ε_{max} = 2.5 normalized by the maximum stress σ_{max} and the maximum strain ε_{max} of each cycle.

4.3.2 Half CTOD length scale ℓ around crack tips

For soft materials, a half CTOD length is comparable with the nonlinear elastic length scale G/E derived from LEFM where G is energy release rate and E is Young's modulus, which were also confirmed for a crack initiation of pre-notched DN gels [6]. **Fig. 4-8** depicts the relationships between G/E and the half CTOD length scale ℓ for each DN sample. Around G_{th}, both length scales showed good correlation for the DN gels showing the suppression of slow mode. On the other hand, for the slow-mode crack propagations of DN(2.0-0.1), this correlation was no longer hold as shown in **Fig. 4-8f**, which implies that the energy dissipation due to the viscoelasticity plays a main role on behalf of a nonlinear elasticity around crack tips during a slow-mode crack propagation.

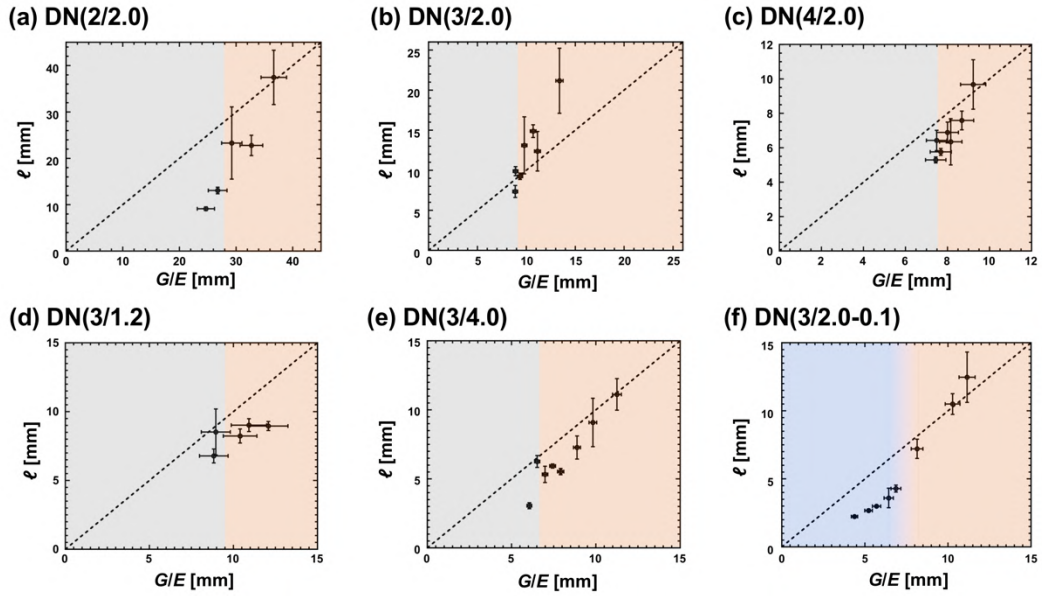

Fig. 4-8. Relationship between the nonlinear elastic length scale G/E and the half CTOD length scale ℓ of each sample.

4.3.3 Relationship between ℓ and energy flux into propagating cracks

Finally, the energy balance of the propagating crack of the DN gel is discussed. In previous work, an energetic measure G_ℓ defined by the half CTOD length scale ℓ was constructed by analogy of LEFM as

$$G_\ell = 2\mu\ell \qquad (4.2)$$

where μ is the plane stress shear modulus obtained by the direct *in situ* measurement of the plane stress longitudinal wave velocity (denoted as c_p^x) along the x line prior to the crack tip [9]. Surprisingly, this value coincided with the energy release rate G for the DN samples in pure shear geometries with a small aspect ratio (the initial heights were < 31 mm and the widths were 70–80 mm), which suggests that the elastic energy derived from the modulus within ℓ from the

crack tip flows into the crack tip and compensates the fracture energy Γ at brittle fracture. In this study, we checked if this balance could be hold for two DN samples; one is the necking DN(3/2.0) that shows only fast mode and the other one is the unnecking DN(3/2.0-0.1) that shows slow mode and fast mode.

The shear moduli μ (MPa) of the two samples were calculated from the Young's modulus obtained by the first loading of the cyclic tensile tests in the range of ε = 0.05–0.15, $E_{\text{p.s.}}$, instead of that by the uniaxial tensile test, E_{uni}, as

$$\mu = E_{\text{p.s.}}/3 \qquad (4.3)$$

since the μ obtained from ${c_{\text{p}}}^{x}$ showed good agreement with $E_{\text{p.s.}}/3$ in the previous work. It should be noted that the biaxial effect for the modulus ($E_{\text{p.s.}} = 4/3 \times E_{\text{uni}}$ [18,20]) failed in this time for some reason (E_{uni} = 0.174 MPa, $E_{\text{p.s.}}$ = 0.433 MPa for DN(3/2.0), and E_{uni} = 0.187 MPa, $E_{\text{p.s.}}$ = 0.400 MPa for DN(3/2.0-0.1)).

Fig. 4-9 depicts the relationship between the bulk energy release rate G and the energetic value G_ℓ. For the necking DN(3/2.0), it was confirmed that $G_\ell > G$, which is contrary to the previous results [9]. However, since the smaller the aspect ratio of the sample is, the G_ℓ increased at given G as reported previously, the large G_ℓ might be reasonable for our samples with smaller aspect ratio (initial heights of 10 mm and the widths of 50 mm). Additionally, the μ, which corresponds to the preserved elasticity along the perpendicular axis to stretch direction, should much decrease from the virgin state at crack propagation due to the large threshold of strain for small aspect ratio sample. Considering it, the real G_ℓ might be lower than the calculated values, which implies that $G_\ell \approx G$ could be also actually hold for DN(3/2.0).

For the unnecking DN(3/2.0-0.1), the same explanation could be adopted

for the fast-mode crack propagation, where $G_\ell \geq G$. On the other hand, only for slow-mode crack propagation, it was confirmed that $G_\ell < G$, which suggests that the bulk stored elastic energy could not be balanced by G_ℓ. We consider the reason why $G_\ell < G$ is that the energy consumption is governed by not only elastic energy flux but also the viscoelasticity around the crack tips as mentioned in **Chapter 3**.

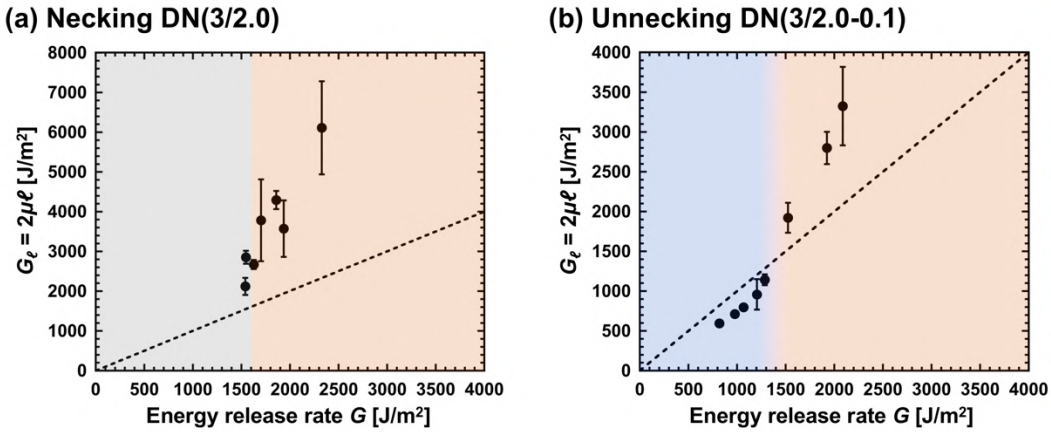

Fig. 4-9. Relationship between the bulk energy release rate G and the energetic measure G_ℓ for (a) necking DN(3/2.0) and (b) unnecking DN(3/2.0-0.1).

4.4 Conclusions

Crack shapes of DN gels with various network structures were systematically studied. We observed the cracks blunting as previously reported and revealed that these obeys the nonparabolic power law of $x = ay^b$ where $b < 2$. We found that the correlation between the crack shape parameter b and the strain-hardening behaviors after damaged by investigating the unloading curves of DN gels obtained by the cyclic tensile tests. We confirmed that the half CTOD length scale ℓ which is calculated from the a and b showed good agreement with the nonlinear elastic length scale G/E for fast-mode crack propagation of the DN gels. The evaluation of the energetic measure G_ℓ defined by the ℓ implies that the elasticity dominates the energy dissipation around crack tip for fast-mode crack propagation while the viscoelasticity might play a role for slow-mode crack propagation of the unnecking DN samples. Further study on the modulus change in perpendicular axis during elongation are expected for more exact quantitative evaluation.

4.5 Reference

[1] A. Livne, E. Bouchbinder, I. Svetlizky, J. Fineberg, The Near-Tip Fields of Fast Cracks, *Science*, 327 (2010) 1359–1363.

[2] T. Goldman, R. Harpaz, E. Bouchbinder, J. Fineberg, Intrinsic Nonlinear Scale Governs Oscillations in Rapid Fracture, *Phys. Rev. Lett.*, 108 (2012) 1–5.

[3] F. Luo, T. L. Sun, T. Nakajima, T. Kurokawa, Y. Zhao, A. Bin Ihsan, H. L. Guo, X. F. Li, J. P. Gong, Crack Blunting and Advancing Behaviors of

Tough and Self-Healing Polyampholyte Hydrogel, *Macromolecules*, 47 (2014) 6037–6046.

[4] Y. Morishita, K. Tsunoda, K. Urayama, Crack-Tip Shape in the Crack-Growth Rate Transition of Filled Elastomers, *Polymer*, 108 (2017) 230–241.

[5] R. Long, C. Y. Hui, J. P. Gong, E. Bouchbinder, The Fracture of Highly Deformable Soft Materials: A Tale of Two Length Scales, *Annu. Rev. Condens. Matter Phys.*, 12 (2021) 71–94.

[6] Y. Zheng, T. Matsuda, T. Nakajima, W. Cui, Y. Zhang, C.-Y. Hui, T. Kurokawa, J. P. Gong, How Chain Dynamics Affects Crack Initiation in Double-Network Gels, *Proc. Natl. Acad. Sci.*, 118 (2021) e2111880118.

[7] A. Livne, E. Bouchbinder, J. Fineberg, Breakdown of Linear Elastic Fracture Mechanics near the Tip of a Rapid Crack, *Phys. Rev. Lett.*, 101 (2008) 1–4.

[8] T. Goldman Boué, R. Harpaz, J. Fineberg, E. Bouchbinder, Failing Softly: A Fracture Theory of Highly-Deformable Materials, *Soft Matter*, 11 (2015) 3812–3821.

[9] I. Kolvin, J. M. Kolinski, J. P. Gong, J. Fineberg, How Supertough Gels Break, *Phys. Rev. Lett.*, 121 (2018) 135501.

[10] J. R. Rice, A Path Independent Integral and the Approximate Analysis of Strain Concentration by Notches and Cracks, *J. Appl. Mech. Trans. ASME*, 35 (1964) 379–388.

[11] G. Ramorino, S. Agnelli, R. De Santis, T. Riccò, Investigation of Fracture Resistance of Natural Rubber/Clay Nanocomposites by J-Testing, *Eng.*

Fract. Mech., 77 (2010) 1527–1536.

[12] S. Agnelli, G. Ramorino, S. Passera, J. Karger-Kocsis, T. Riccò, Fracture Resistance of Rubbers with MWCNT, Organoclay, Silica and Carbon Black Fillers as Assessed by the J-Integral: Effects of Rubber Type and Filler Concentration, *Express Polym. Lett.*, 6 (2012) 581–587.

[13] C. Liu, H. Kadono, H. Yokoyama, K. Mayumi, K. Ito, Crack Propagation Resistance of Slide-Ring Gels, *Polymer*, 181 (2019) 121782.

[14] R. Long, C. Y. Hui, Crack Tip Fields in Soft Elastic Solids Subjected to Large Quasi-Static Deformation - A Review, *Extrem. Mech. Lett.*, 4 (2015) 131–155.

[15] Y. Zhang, K. Fukao, T. Matsuda, T. Nakajima, K. Tsunoda, T. Kurokawa, J. P. Gong, Unique Crack Propagation of Double Network Hydrogels under High Stretch, *Extrem. Mech. Lett.*, 51 (2022) 101588.

[16] T. Nakajima, T. Kurokawa, S. Ahmed, W. Wu, J. P. Gong, Characterization of Internal Fracture Process of Double Network Hydrogels under Uniaxial Elongation, *Soft Matter*, 9 (2013) 1955–1966.

[17] J. P. Gong, Why Are Double Network Hydrogels so Tough?, *Soft Matter*, 6 (2010) 2583–2590.

[18] T. T. Mai, T. Matsuda, T. Nakajima, J. P. Gong, K. Urayama, Distinctive Characteristics of Internal Fracture in Tough Double Network Hydrogels Revealed by Various Modes of Stretching, *Macromolecules*, 51 (2018) 5245–5257.

[19] K. Fukao, T. Nakajima, T. Nonoyama, T. Kurokawa, T. Kawai, J. P. Gong, Effect of Relative Strength of Two Networks on the Internal

Fracture Process of Double Network Hydrogels As Revealed by *in Situ* Small-Angle X-Ray Scattering, *Macromolecules*, 53 (2020) 1154–1163.

[20] B. Yohsuke, K. Urayama, T. Takigawa, K. Ito, Biaxial Strain Testing of Extremely Soft Polymer Gels, *Soft Matter*, 7 (2011) 2632–2638.

Chapter 5: Summary of the dissertation

In this dissertation, we have reported the unique crack propagation behaviors of DN gels in highly stretched state. The post-notching crack growth test enables us to extract many profiles of the crack propagations, such as the velocity of crack growth, the birefringence distribution, and the crack shape, over wide range of energy release rate. And these results have given insights to elucidate the crack propagation mechanism of DN gels.

In **Chapter 3**, we systematically investigated the power-law relationship between the energy release rate G and the velocity of crack growth v. As a result, we confirmed the strong correlation between the uniaxial tensile behaviors and the crack propagation behaviors of DN gels. As well as rubber materials, the SN gel and the unnecking DN gels shows the velocity jump phenomena at the critical energy release rate G_{jump}. On the other hand, the necking DN gels show not only the significantly high threshold of energy release rate for crack propagation, G_{th}, but also the ability to suppress the slow-mode crack propagation, which indicates that the necking DN gels have great and unique crack resistance. Birefringence measurements revealed that a large damage zone in millimeter scale is formed around the crack tip at $G < G_{\mathrm{th}}$, which well agreed with the previously proposed model for the explanation of the high fracture energy of DN gels. We also verified that the damage zone weakens once the crack propagates at $G > G_{\mathrm{th}}$, which implies that the insufficient time for the network deformation to form the damage zone results in the acceleration of the crack growth at crack initiation.

In **Chapter 4**, we systematically investigated the crack shape profiles of DN gels. We demonstrated that the crack shapes of DN gels obeys $x = ay^b$ where b is lower than 2, which indicates that the crack blunting occurs in DN gels, and the crack propagation mechanism of DN gels cannot be explained by conventional fracture models. We also found that the crack shape parameter b is affected by the steepness of the strain-hardening behaviors after samples are damaged, which suggests that the contrast of the strength of the two networks causes the unique crack shapes of DN gels. Calculating the half CTOD length scale ℓ from a and b enables the quantitative discussion on how the energy is balanced around the crack tips, which implies that the strong nonlinear elasticity might dominate the energy consumption during fast-mode crack propagations in DN gels.

This dissertation discovered the unique crack resistance of DN gels for the first time. Furthermore, it proposed the crack propagation mechanism not only at crack initiation but also at brittle fracture where polymer physics are dominated by extremely high frequency, which has been never discussed previously for DN gels. We believe that the studies in this dissertation are helpful for a design of novel materials with great crack resistance. In addition, we also believe that it will facilitate further studies for completely understanding of fracture mechanism of DN gels.

List of Publications

Original papers related to doctoral dissertation

1. Y. Zhang, K. Fukao, T. Matsuda, T. Nakajima, K. Tsunoda, T. Kurokawa and J. P. Gong, Unique Crack Propagation of Double Network Hydrogels under High Stretch, *Extreme Mechanics Letters* 51 (2022), 101588.

Other papers

1. Y. Zheng, T. Matsuda, T. Nakajima, W. Cui, Y. Zhang, C.-Y. Hui, T. Kurokawa, J. P. Gong, How Chain Dynamics Affects Crack Initiation in Double-Network Gels, *Proc. Natl. Acad. Sci.*, 118 (2021) e2111880118.

Presentations in conferences related to doctoral dissertation

1. Y. Zhang, K. Fukao, T. Matsuda, T. Nakajima, K. Tsunoda, T. Kurokawa and J. P. Gong, “大変形下におけるダブルネットワークゲルの特徴t系な亀裂進展挙動”, 第33回高分子ゲル研究討論会, online, January 2022 (Oral).
2. Y. Zhang, K. Fukao, T. Matsuda, T. Nakajima, K. Tsunoda, T. Kurokawa and J. P. Gong, “ダブルネットワークゲルにおける進展亀裂の高分子鎖ダイナミクス”, 第31回日本MRS年次大会, online, December 2021 (Poster).
3. Y. Zhang, K. Fukao, T. Matsuda, T. Kurokawa, T. Nakajima, K. Tsunoda and J. P. Gong, “Analysis of Crack Propagation of Double Network Gels”, Strasbourg-Hokkaido Symposium, Strasbourg (France), November 2019 (Oral).

4. Y. Zhang, K. Fukao, T. Matsuda, T. Kurokawa, T. Nakajima, K. Tsunoda and J. P. Gong, “ダブルネットワークゲルの耐亀裂性向上化機構の解明”, 第9回CSJ化学フェスタ2019, Tokyo (Japan), October 2019 (Poster).
5. Y. Zhang, K. Fukao, T. Matsuda, T. Kurokawa, T. Nakajima, K. Tsunoda and J. P. Gong, “Specific Crack Propagation Behaviors of Double Network Gels”, ゲルワークショップ イン 福井, Fukui (Japan), October 2019 (Poster).
6. Y. Zhang, K. Fukao, T. Matsuda, T. Kurokawa, T. Nakajima, K. Tsunoda and J. P. Gong, “ダブルネットワークゲルが有する特徴的な亀裂進展挙動”, 第68回高分子討論会, Fukui (Japan), October 2019 (Oral).
7. Y. Zhang, K. Fukao, T. Matsuda, T. Kurokawa, T. Nakajima, K. Tsunoda and J. P. Gong, “Crack Propagation Behaviors of Double Network Gels”, The 10th Graduate School of Chemical Sciences and Engineering (CSE) and Ambitious Leader’s Program (ALP) International Summer School, Sapporo (Japan), July 2019 (Poster).
8. Y. Zhang, K. Fukao, T. Matsuda, T. Kurokawa, T. Nakajima, K. Tsunoda and J. P. Gong, “ダブルネットワークゲルの耐亀裂性評価”, 第53回（2018年度）高分子学会北海道支部研究発表会, Chitose (Japan), January 2019 (Oral).
9. Y. Zhang, K. Fukao, T. Matsuda, T. Kurokawa, T. Nakajima, K. Tsunoda and J. P. Gong, “ダブルネットワークゲルの亀裂進展挙動の解析”, 第67回高分子討論会, Sapporo (Japan), August 2018 (Poster).
10. Y. Zhang, K. Fukao, T. Matsuda, T. Kurokawa, T. Nakajima and J. P.

Gong, “Evaluation of the Fracture Dynamics of DN gels”, The 5th International Symposium on Ambitious Leader’s Program Fostering Future Leaders to Open New Frontiers in Materials Science, Sapporo (Japan), November 2017 (Poster).

11. Y. Zhang, K. Fukao, T. Matsuda, T. Kurokawa, T. Nakajima and J. P. Gong, “DNゲルの破壊ダイナミクスの評価”, ImPACT伊藤プログラム第3回若手研究会, Shonan (Japan), October 2017 (Poster).
12. Y. Zhang, K. Fukao, T. Matsuda, T. Kurokawa, T. Nakajima and J. P. Gong, “DNゲルの破壊靭性評価法の確立”, 2017年度北海道高分子若手研究会, Sapporo (Japan), September 2017 (Poster).

Acknowledgement

This researches has been carried out in Laboratory of Sof & Wet Matter (LSW), Graduate School of Life Science, Hokkaido University, Japan, and it would have been impossible to do without a lot of supports that I received from many people.

Firstly, I greatly appreciate all the supports of my supervisor, Professor Jian Ping Gong. Her inquisitive nature and enjoying attitude to science always encouraged my motivation for the experiments and researches through many supportive discussions. I also really appreciate her thoughtful mind and generous heart. She gave me a lot of tolerant supports and lessons for not only academic occasions but also my private life, which considerably made my school life enjoyable. There is no doubt that I would not have been able to complete my research without her, and I would like to thank her again.

I am also gratful to Professor Takayuki Kurokawa, Associate Professor Tasuku Nakajima, Associate Professor Takayuki Nonoyama, Assistant Professor Daniel R. King, Assistant Professor Kunpeng Cui, Assistant Professor Hailong Fan, and Associate Professor Tsutomu Indei for their valuable discussions, useful suggestions for my academic researches I also appreciate Katsuhiko Tsunoda in Bridgestone corporation, who gave taught me a lot of indispensable advices and suggestions for my doctoral research.

I also would like to thank post-doctoral fellows, guest researchers, research assistants and administrative staffs in LSW. Especially, Dr. Yoshinori Katsuyama

helped me a lot by technical supports to product equipment for my researches. I also would like to thank the staffs in LSW; Ms. Eiko Hasegawa, Ms. Yuki Okubo, Ms. Iseya, and Ms. Kamada for helping me.

I also would like to say many thanks to the student members in LSW for their helpful and kind attitude in daily life. They made my life in hokkaido happy many time throuout sightseeing trips or drinking parties. Especially, I want to thank Tsuyoshi Okumura, who is in the same grade with me and a good friend, for helping and caring me in many occasions.

I want to gratefully acknowledge Hokkaido University's "Ambitious Leader's Program" supported by MEXT, Japan for supporting my research with its financial support and fruitful opportunity. It taught me not only academic skills, but also a variety of things that I will need to be active in the international society in the future.

Finally, grateful thanks to my family for all the supports during the life in Hokkaido University. I dedicate this dissertation to them.

Ye Zhang
Laboratory of Soft & Wet Matter
Graduate School of Life Science
Hokkaido University
Sapporo Japan
March 2022